
Expedition 314 Site C0003¹

Expedition 314 Scientists²

Chapter contents

Background and objectives	1
Operations	1
Data and log quality	3
Log characterization and lithologic interpretation	4
Physical properties	5
Structural geology and geomechanics	7
Log-seismic correlation	7
Discussion and synthesis	10
References	10
Figures	11
Tables	40

Background and objectives

Integrated Ocean Drilling Program Site C0003 (proposed Site NT2-01D) is located on the lower slope off Kii Peninsula, just seaward of the Kumano forearc basin. The Site C0003 summary log diagram is shown in Figure F1.

Goals at proposed Site NT2-01 included logging while drilling (LWD) of ~1000 m of the midslope region, across at least one major strand of the megasplay fault system (Fig. F2). This proposed site was intended to begin the downdip transect of the megasplay fault system by sampling a relatively shallow, presumably aseismogenic point on the fault zone at ~800 meters below seafloor (mbsf). The anticipated lithology was deformed terrigenous sediment, faults, and possible gas hydrate, though there is no clear bottom-simulating reflector at this site. Beneath the near-surface slope deposits, the acoustically transparent zone above the reflective thrust fault was predicted to be composed of highly deformed and faulted accretionary mélange and/or disrupted stratigraphy of slope deposits. Beneath the fault reflector, three-dimensional (3-D) seismic data suggested drilling would penetrate deformed but stratigraphically intact slope sediments overridden by the splay thrust fault.

Unfortunately, we encountered very difficult drilling conditions at Site C0003, such as especially pronounced caving and washout of likely fault zones and possibly sandy intervals, which caused the drill string to become irretrievably stuck before reaching the primary objective. We lost a complete LWD tool string and ~200 m of drill collars at this site. Nevertheless, real-time data transmission provided substantial logging data from the seafloor to ~530 m LWD depth below seafloor (LSF). This incident prompted the decision to add another site (C0004) in order to drill through the shallower part of the megasplay fault zone to meet the primary objective (see the “[Expedition 314 Site C0004](#)” chapter for details).

Operations Hole C0003A

Hole C0003A was spudded at 1300 h on 20 October 2007. LWD-measurement-while-drilling (MWD) operations were conducted from the seafloor (2481.5 m drillers depth below rig floor [DRF]) to a total depth of 3007 m DRF (525.5 m LSF), where the drill pipe became stuck and pipe connection was lost. In spite of numerous

¹Expedition 314 Scientists, 2009. Expedition 314 Site C0003. In Kinoshita, M., Tobin, H., Ashi, J., Kimura, G., Lallemand, S., Screaton, E.J., Curewitz, D., Masago, H., Moe, K.T., and the Expedition 314/315/316 Scientists, *Proc. IODP, 314/315/316*: Washington, DC (Integrated Ocean Drilling Program Management International, Inc.). doi:10.2204/iodp.proc.314315316.115.2009

²[Expedition 314/315/316 Scientists' addresses.](#)



efforts to recover the bottom part of the bottom-hole assembly (BHA) (including the MWD-annular pressure while drilling [APWD]-LWD tools), the fishing operation was not successful and the hole was cemented on 30 October, leaving the tools behind. The summary of operations in Hole C0003A is shown in Table T1, and a schematic of the final hole condition at the time of plugging and abandonment is shown in Figure F3.

In detail, operations began with making up the BHA (at 2300 h on 18 October), tool initialization, calibration, and shallow (36.8 m DRF) communication tests (at 1830 h on 19 October). The BHA included a polycrystalline diamond bit, various subs, LWD tools, one mechanical jar, twenty 6¾ inch drill collars (12 below the jar and 8 above the jar), and an extra crossover sub to connect the BHA to the drill pipe (Table T2). As with Hole C0002A, the LWD tools (6¾ inch [17.15 cm] collars) included, from bottom to top, the geoVISION tool with a 23.18 cm button sleeve, the sonicVISION (four-receiver array) tool, the MWD (PowerPulse) tool, the seismicVISION tool, and the adnVISION tool (see Fig. F1 in the “Expedition 314 methods” chapter). Installing the radioactive source for density measurement was completed at 2100 h on 19 October, and the BHA was lowered to run into hole. Communication with all tools and function checks were conducted again at 348 m DRF between 2330 and 2345 h on 19 October. After the end of the dynamic positioning system calibration operation, the seafloor was tagged at 2481.5 m DRF (2453 m mud depth below sea level [MSL]) and hole position was confirmed and surveyed by the remotely operated vehicle (ROV) (at 1145 h on 20 October) (Table T1). At ~6 m above seafloor (from 1150 to 1210 h on 20 October), the surface air gun array was activated and the seismicVISION tool was tested again. Real-time data were of poor quality because of poor fluid pulse telemetry efficiency in the noisy environment caused by pipe vibration in the strong current. Hole C0003A was jetted-in at 1245 h on 20 October with an initial pump rate of 500–650 gpm to ~50 m LSF. Real-time communication with the tools was initially poor, as the pumping rate was limited in this jet-in interval to reduce washout. A graphic representation of the drilling parameters and gamma ray log is given in Figure F4. As the LWD tools were not recovered, only real-time data were ultimately available.

Below 50 m LSF, drilling progressed smoothly at a constant rate of penetration (ROP) of 35 m/h. Collar (bit) rotation speed (CRPM) progressively increased from 30 to 80 rpm at 80 m LSF to reach a constant value of 100 rpm until the end of operation. Pump flow increased to 650–680 gpm and standpipe pres-

sure (SPPA) was maintained at 15 MPa (normal trend increase with depth to 18 MPa at 525 m LSF). Standard pipe connection procedure included circulation, hole sweep, and pumping high-viscosity gel. Surface weight on bit was kept to a minimum to 490 m LSF, where the first significant increase in equivalent circulating density (ECD)/APWD and torque were noticed (at 1000 h on 21 October). The hole was reamed at 8 m depth intervals until the tool string became stuck (at 1310 h on 21 October; 525.5 m LSF). While attempting to increase circulation and work the stuck pipe loose, the drill pipe broke at 1350 h, detected by the loss of ~10 tons of string weight.

A free-fall funnel was dropped, and the remaining string was pulled out of the hole at 0230 h on 22 October. After recovering the drill string, it was observed that 19 of the 20 drill collars and the entire LWD BHA assembly had been lost. The second to last pipe recovered on deck was plugged with cuttings and large pieces of mudstone and sandstone, and the bottom drill pipe threads were heavily damaged. After repair of a deformed 8½ inch overshot guide, a fishing assembly was made up, run in, reentered, washed down, and reamed from 2707 to 2785 m DRF. Between 0000 and 0745 h on 24 October, fishing was attempted seven times with one successful catch; however, the fishing tool failed to pull up. Therefore, it was pulled out to the rig floor at 1415 h on 24 October and run again with a 6¾ inch grapple assembly on 25 October. Reentry to the well was difficult and took 10 h to get into the hole. The overshot again failed to catch the fallen LWD assembly, and the decision was made to deploy a wireline fishing tool to retrieve the radioactive source from the adnVISION tool. The wireline was rigged up for a “dummy run” with a 7 m sinker bar instead of a fishing tool for the radioactive source at 2215 h on 25 October. After failing to pass through 2780.5 m DRF at 0145 h on 25 October, the dummy tool was retrieved. However, the sinker bar had unscrewed and dropped off, possibly into the hole. The overshot assembly was pulled out of the hole and recovered on deck at 0000 h on October 27.

After the overshot assembly was pulled out of the hole at 0000 h on 27 October, the D/V *Chikyu* sailed 14 nmi north-northwest to move away from the strong current and a typhoon. At 1600 h on 27 October the *Chikyu* sailed back to Hole C0003A and an 8½ inch overshot assembly with 6½ inch spiral grapple. After moving 6 nmi upstream, the overshot assembly began running into the water to 1800 m DRF, and the ROV dived while drifting back to position. The hole was reentered at 0315 h on 28 October and run in to 2774 m. Wireline equipment was rigged up at 0600 h and the

overshot latched the pipe after several attempts. An attempt to pass the wireline past 2788 m DRF failed, and it was finally decided to rig down the wireline equipment at 1530 h. Fishing with the overshot continued until the decision was made to pull out at 1200 h on 29 October.

At 1900 h, the *Chikyu* sailed 500 m upstream and made up a cement stinger. The cement stinger was run in beginning at 2000 h, and a cement stand was rigged up and cement lines flushed at 0230 h on 30 October. After testing pressure, the first cement job was conducted at 0430 h and the drill string was displaced with seawater. A second cement job was conducted at 0730 h after pulling out from 2760 to 2612 m DRF. Seawater again was displaced and cement returned to the seabed was confirmed by ROV. After cementing, the cementing assembly was pulled out of the hole, the ROV was recovered, and the drill string was cleaned.

Transit to Site C0004

After picking up the beacons from Site C0003, the *Chikyu* moved to the proposed Site NT2-011 pilot hole location at 0330 h on 31 October 2007 with ROV and beacons in the water for 1 nmi at an average speed of 0.3 kt. The four beacons were set and calibrated until 1740 h. The ship then moved 4 nmi upstream at 1740 h with average speed of 2.4 kt and drifted back to the location at 2140 h at 1.3 kt.

Data and log quality

Hole C0003A

Available data

Hole C0003A was drilled with LWD-MWD-APWD tools. Similar to Hole C0002A, all MWD-APWD data and a limited set of LWD data were transmitted in real time. As the tools were not recovered (see “[Operations](#)”), these real-time data are the only data available for this site. In addition to surface and downhole drilling parameter logs, this data set includes the following main geophysical logs:

- Bulk density (RHOB_DH) and bulk density correction (DRHO_DH) computed downhole with a less sophisticated algorithm than the one normally used at the surface with the memory data;
- Thermal neutron ratio (TNRA_ADN_RT) and thermal neutron porosity (TNP_H_ADN_RT);
- Average borehole diameter from the ultrasonic caliper (ADIA);
- Natural gamma ray log (GR) and resistivities (bit [RES_BIT_RT] and ring [RES_RING_RT], shallow [RES_BS_RT], medium [RES_BM_RT], and deep

[RES_BD_RT] button) from the geoVISION resistivity (GVR) tool;

- Hole deviation data such as relative bearing (RB_RT), hole azimuth (HAZI_RT), and hole deviation (DEVI_RT); and
- Δt compressional wave transit time (DTCO) and sonic compressional semblance (CHCO) and semblance (DTCO and CHCO) from the sonicVISION tool (see Table T2 in the “Expedition 314 methods” chapter).

Depth shift

As Hole C0003A was jettied-in to 50 m LSF at a reduced pump rate, real-time fluid pulse data were available only while the bit was below 50 m LSF. Therefore, geoVISION data are available from ~50 m LSF (Fig. F5, yellow zone), whereas adnVISION data (sensors located ~27–29 m above) are available from ~22 m LSF (Fig. F5, orange zone). Therefore, the mudline was impossible to identify based on a first response in the gamma ray (GR) log and so was picked at 2481.5 m DRF. The depth-shifted version of the main drilling data and geophysical logs in Hole C0003A is given in Figure F5. Figure F6 presents the time-depth relationship linking the time (Fig. F4) and depth version (Fig. F5) of the data in Hole C0003A.

Logging data quality

Figure F5 shows the quality control logs for Hole C0003A real-time LWD data. After the hole was jettied-in to 50 m LSF, the target ROP of 35 m/h was generally achieved to 525.5 m LSF, where loss of the BHA stopped drilling operations (see “[Operations](#)”). Below 50 m LSF, SPPA slightly increased from 15 to 18 MPa. CRPM also progressively increased from 30 to 50 rpm, then 80 rpm, and stabilized at 100 rpm below 190 m LSF. Average annular pressure and ECD followed the normal trend of increasing with depth with moderate jumps at pipe connections. Even though not perfectly calibrated (negative temperature value above 280 m LSF), annular temperature (ATMP_MWD) shows a normal increase with depth until the tool became stuck and pump flow increased.

Based on previous experience in Hole C0002A, drilled with a similar ROP, time after bit (TAB) measurements were ~5 min for resistivity and gamma ray logs (geoVISION tool), except in short depth intervals corresponding to pipe connections. TAB measurements for density and neutron porosity logs are ~45–60 min. The real-time acoustic caliper (ADIA) log, which gives the average diameter of the LWD borehole, is the best indicator of borehole condi-

tions. The ECAL_RAB caliper is a resistivity-derived caliper. In comparison to the ADIA, it has the advantage of providing a caliper reading shortly after the hole has been drilled, but its physical foundation (resistivity derived) is less reliable than the acoustic reading (relying only on drilling fluid sound velocity). The ADIA caliper should read a value of 8.5 inches (21.6 cm) for a perfect in-gauge hole but instead showed values slightly >9 inches for the depth interval from 30 (first reading) to 75 m LSF and slightly <9 inches (22.9 cm) for the depth intervals 155–390 and 460–525.6 m LSF. ADIA exceeds 10 inches in a low-gamma ray zone (sandy formation; 75–155 m LSF). ADIA also shows a complex wash-out/bridge pattern between 390 and 460 m LSF that is not concomitant to any change in gamma ray value (lithology indicator) and was therefore interpreted as the result of a fault zone. Hole deviation never exceeded 3°. LWD tools experienced moderate radial and tangential shocks. The highest shocks (SHKPK) correspond to the lower section of the sand-rich interval (110–155 m LSF) where the stick-slip indicator (STICK) gradually increased to 450 m LSF, where it reduced and stabilized to a value of 150 rpm (far below the 250 rpm limit that can impair image quality and therefore also far below the maximum rating of the tool).

The washouts in the interpreted fault zone and, more specifically, in the upper sand-rich interval are associated with major decreases in the bulk density log (RHOB) where bulk density correction (DRHO) could not be fully compensated for this major wash-out and are therefore underestimated (Fig. F5). Otherwise, a stand-off <1 inch (2.5 cm) between the tool and the borehole wall indicates high-quality density measurements with an accuracy of ± 0.015 g/cm³. Comparison between deep button (RES_BD) and shallow button (RES_BS) resistivity values shows that drilling fluid invasion is null or not significant, confirming the short TAB readings.

Because of the loss of the LWD tools, sonic data are limited to real-time downhole automatic picking of compressional arrival time (DTCO) and coherence (CHCO) information. The full waveforms were not available, limiting further processing and detailed quality check. However, interval velocity data derived from the real-time check shot show a surprisingly good fit with the upper limit of V_p data derived from DTCO from 162 to 523 m LSF (see “[Log-seismic correlation](#)”).

Log characterization and lithologic interpretation

Log characterization and identification of logging units

In Hole C0003A only real-time data were available because of the loss of the LWD drill collars. Data are available to a maximum depth of 532 m LSF, including gamma ray; ring, bit, and deep resistivity; neutron porosity; and density log responses. Because of the poor quality of the sonic log (see “[Data and log quality](#)”), it was not used to define the logging units. The top ~55 m LSF of data for all the logs was discarded because of poor sampling. Three logging units (Table T3; Fig. F1) were defined based on the variability of the available log responses. Statistical analysis supported the differences among these units (Fig. F7).

Logging Unit I (55–76.6 m LSF) is characterized by a moderately high gamma ray baseline (50–55 gAPI) with high variability across this baseline. All three resistivity responses are similar and remain fairly constant (~ 0.9 Ω m). The density and neutron responses are moderately high (~ 1.6 g/cm³ and 60 porosity units, respectively), with minor fluctuations. The caliper indicates that the borehole quality is poor (9.5–11.5 inches), and this may explain some of the variation observed in the density and neutron log responses.

The base of logging Unit I (76.6 m LSF) is a prominent boundary characterized by a sharp drop in gamma ray, resistivity, and density baseline values and an increase in neutron baseline values. These log responses correspond to a sharp decrease in borehole quality. Logging Unit II (76.6–151.5 m LSF) is characterized by very low gamma ray values (~ 30 gAPI) with meter-scale variations. The resistivity responses are consistently low (0.65 Ω m), with sporadic positive peaks. The measured density is low (~ 1.2 g/cm³) and highly variable, which correlates with the continuously poor borehole quality. The base of logging Unit II is characterized by a sharp increase in all the log responses, accompanied by a return to good borehole conditions.

Logging Unit III (151.5–509 m LSF) exhibits a broad increasing trend in the gamma ray log (average = 77 gAPI), whereas the resistivity profiles (average = 1.65 Ω m), density (average = 1.9 g/cm³), and neutron (55–65 porosity units) log responses remain fairly con-

stant. Subtle internal variation is exhibited throughout logging Unit III. The gamma ray log exhibits high-frequency (meter scale) and high-amplitude variations. The resistivity and density logs exhibit relatively constant values with local negative peaks, usually corresponding to washouts indicated by the caliper and low gamma ray values.

Log-based lithologic interpretation

Logging Unit I (slope sediments)

Within the 21.6 m section of logging Unit I, moderate gamma ray, low resistivity, and low density log values suggest a lithology of mud with interbeds of sandy and silty sediments. Logging Unit I corresponds to the base of a sequence of slope sediments seen in the seismic section (see [“Log-seismic correlation”](#)).

Logging Unit II (thrust sheet)

Logging Unit II is defined by a washed out zone, characterized by low gamma ray and resistivity values. Shipboard correction of the gamma ray log (applying LWD GR hole size correction [GR-4 Schlumberger chartbook, Schlumberger 1995]) was performed to investigate the possibility of borehole effects causing the low gamma ray measurements. The gamma ray values corrected for actual borehole diameter using the real-time caliper are still low (average = 32 gAPI). This range of low gamma ray values is typical for coarse sediments, most likely sandy, uncemented (washed out and low density), and porous (low resistivity formation).

Logging Unit III (thrust sheet)

When compared to logging Units I and II, logging Unit III displays overall higher gamma ray values increasing with depth, increased density, and higher resistivity values. The most likely lithologic interpretation is clay-rich sediment showing no significant compaction trend with depth.

Six washed out intervals (Table T4; Fig. F8) identified within this unit are considered as potential deformation-related zones and display distinctive log responses. Within these intervals, changes in density and resistivity values might be caused by changes in physical properties along zones of deformation, as recognized in the seismic data (see [“Structural geology and geomechanics”](#) and Fig. F9). One of these intervals (415.7–450.5 m LSF) is characterized by very poor quality caliper and corresponding low density and high neutron porosity values. The resistivity and gamma ray logs exhibit very little change across this zone. This area of washout is coincident with a fault zone interpreted in the seismic profiles

(see Fig. F9). Internal subtle changes in gamma ray trends are correlatable with washouts.

A comparison of gamma ray values between Expedition 314 sites and Ocean Drilling Program (ODP) Site 808 is shown in Figure F10. Gamma ray values in logging Unit II are exceptionally low. The values in this unit are also lower than logging Unit 1 at Site 808, which is composed of sand and silt turbidites (Mikada, Becker, Moore, Klaus, et al., 2002).

Physical properties

The loss of the BHA in Hole C0003A required the use of only MWD and data acquired in real time for our analyses. Data available for physical property analyses were neutron porosity (TNUC, thermal neutron porosity ultrasonic caliper corrected), bulk density (RHOB), three different resistivity logs (bit, ring, and deep button), and two different caliper logs (ADIA and ECAL). ADIA caliper is part of the adnVISION tool and is based on ultrasonic traveltime; ECAL is a less direct measurement based on the difference between shallow and medium button resistivity readings with an assumption of mud (borehole fluid) resistivity. When both calipers are reliable, time-delayed hole washouts can be detected because the ADIA reads caliper from 40 to 60 min after the ECAL does. DTCO was also available for sonic *P*-wave velocity analysis; however, the data quality turned out to be so poor that no meaningful analysis was possible (see [“Log-seismic correlation”](#) for a brief description of the sonic log). As at previous sites, additional analyses were conducted to produce different porosity derived from density and resistivity. Accordingly, estimations of temperature and formation factor were carried out.

Density

The RHOB log is strongly affected by hole conditions, as indicated by caliper data (Fig. F11). Bulk density values in high-caliper intervals are highly underestimated and should not be considered reliable.

The density log averages ~ 1.6 g/cm³ in the uppermost sediments and in logging Unit I, except for the two spikes to 1.41 g/cm³ at 37.5 m LSF and 1.32 g/cm³ at 45.5 m LSF. These spikes are probably caused by hole washouts, as caliper data suggest. Measured density drops from ~ 1.6 g/cm³ at 74 m LSF to ~ 1.2 g/cm³ at 79 m LSF at the boundary between logging Units I and II. In Unit II the density values decrease from ~ 1.25 to ~ 1.10 g/cm³, which is far too low to represent the formation density. These low values are associated with high caliper values and indicate serious

hole enlargement in this zone. Near the top of Unit III (155.9 m LSF), density is 2.00 g/cm^3 . In this unit the density log shows a nearly constant value of $\sim 1.93 \text{ g/cm}^3$ from ~ 152 to 381 m LSF , with some low density spikes related to high caliper (e.g., 247.8–251.9 and 300.5–302.6 m LSF). Below 381.0 m LSF the caliper value significantly increases again, resulting in unreliably low density measurements. These high-caliper zones could be fault-related damage regions. Zones with low caliper values produce higher density values (e.g., 402.0–415.7, 450.5–467.7, and 469.6–489.4 m LSF). Intervals with high density may indicate zones of enhanced compaction or less pervasive disruption by faulting and/or fracturing.

Density-derived porosity

Figure F12 shows a comparison of the two available calipers (ECAL and ADIA), the neutron porosity, and the density-derived porosity calculated from the RHOB log (see the “Expedition 314 methods” chapter). A more systematic comparison of those two porosities was made through cross-plotting (Fig. F13). Those figures show that in logging Unit I, the density-derived porosity log is near constant (65%) and is higher than the neutron porosity log by as much as 10%. In logging Unit II, the few data available are not considered reliable because both of the calipers show values higher than 10 inches. In logging Unit III, the density-derived porosity is almost constant ($\sim 45\%$) and is systematically lower than the neutron porosity by 10%, except for one distinct zone from 470 to 493 m LSF, where the density-derived porosity is close to 35%, and one zone of washouts from 415 to 450 m LSF, where the neutron porosity becomes higher.

Neutron porosity

The TNUC log in Hole C0003A shows scatter throughout the entire depth range (Fig. F14). Both raw data and smoothed data using a 4.5 m running average are presented. Overall, the neutron porosity is nearly constant with depth within each logging unit. The ADIA data show severe washouts in logging Units I, II, and in the bottom part of Unit III. The porosity is likely overestimated in such high-caliper zones.

The porosity log shows a nearly constant value of $\sim 58\%$ in logging Unit I and above and increases sharply from 54.8% at 74 m LSF to 65.9% at 78 m LSF at the boundary between logging Units I and II. In logging Unit II the porosity is nearly constant with depth and is characterized by slight long-wavelength variations with values ranging from $\sim 62\%$ to $<70\%$. These values are probably strongly affected by the poor hole quality. The sharp cutoff of

porosity values $<70\%$ reflects an artificial threshold in the data acquisition. Porosity drops from 68.5% at 148 m LSF to 50.5% at 154 m LSF at the boundary between logging Units II and III. The porosity remains nearly constant with some small fluctuations, ranging between $\sim 47.5\%$ and $\sim 56\%$ above 381 m LSF in logging Unit III. Below 381 m LSF where caliper values are relatively high, the porosity log exhibits fluctuations ranging from $\sim 46\%$ to $\sim 61\%$. However, those values may not be reliable because of washouts.

Resistivity and estimated porosity

Resistivity logs

Figure F15 shows three different resistivity measurements: ring, bit, and deep button resistivity. The overall downhole trends are identical for the three logs. Superposition of the bit and ring resistivity measurements shows very good agreement between them in logging Unit III and for the few data points of logging Unit I and above. In logging Unit II the ring resistivity is significantly lower than the bit resistivity by as much as $0.2 \text{ } \Omega\text{m}$ but this corresponds to a zone of major washout shown by both ECAL and ADIA calipers. This is confirmed by the cross-plot between bit and ring resistivity (Fig. F16). The difference between those two measurements is small in logging Unit III.

The following description of resistivity is based on the bit resistivity shown in Figure F15. Very few resistivity values in logging Unit I and above are reliable. At the bottom of this section (from 55 to 76.6 m LSF) we can distinguish a constant resistivity value of $0.9 \text{ } \Omega\text{m}$. In logging Unit II, the bit resistivity measurement, which should be the measurement least affected by washouts, slightly increases from 0.9 to $1.1 \text{ } \Omega\text{m}$. The logging Unit II/III boundary is marked by a sharp increasing step of resistivity from 1.1 to $1.8 \text{ } \Omega\text{m}$, followed by a decreasing step from 1.8 to $1.6 \text{ } \Omega\text{m}$. From 152 to 320 m LSF, the resistivity data show a near-constant value of $1.6 \text{ } \Omega\text{m}$. At 320 m LSF, we observed a small decreasing step from 1.6 to $1.5 \text{ } \Omega\text{m}$. It is followed, from 330 to 420 m LSF, by an increasing trend of resistivity from 1.5 to $1.7 \text{ } \Omega\text{m}$, and from 420 m to 460 m LSF by a decreasing trend of resistivity from 1.7 to $1.3 \text{ } \Omega\text{m}$, which corresponds to the fractured zone identified in “Log characterization and lithologic interpretation.” Below 460 m LSF, two zones of relatively high resistivity values ($1.7 \text{ } \Omega\text{m}$ between 475 and 485 m LSF and $1.5 \text{ } \Omega\text{m}$ between 505 and 507 m LSF) depart from a trend of constant resistivity values of $\sim 1.5 \text{ } \Omega\text{m}$.

Estimation of temperature profile

The temperature gradient was estimated from porosity-dependent rock thermal conductivity. The depth-

dependent thermal conductivity (K) at this site was obtained using the following equation:

$$K = K_g^{1-\phi} K_w^\phi,$$

where K_g is the grain thermal conductivity (2.85 W/[m·K] from ODP Leg 190 Site 1173 [Moore, Taira, Klaus, et al., 2001]), K_w is the water thermal conductivity (0.60 W/[m·K]), and ϕ is the thermal neutron porosity. Calculated K is ~1.0 W/(m·K) in logging Unit I and II and ~1.3 W/(m·K) in logging Unit III. Surface temperature of 2°C and surface heat flow of 60 mW/m² were assumed. The resulting temperature reaches 28°C at 535 m LSF.

Estimation of porosity from resistivity

The seawater electrical resistivity was calculated as a function of temperature (see the “[Expedition 314 methods](#)” chapter) and used to evaluate both ring and bit formation factors. Ring and bit formation factors are normally related to porosity by Archie’s law. Formation factor versus density and porosity cross-plots (Fig. F17) show that the data points from logging Units I (and above) and III fit well to an Archie’s law curve, with $a = 1$ and $m = 2.4$. The resistivity-derived porosity profiles were then calculated with these parameters. It should be noted that lithologic variations, not taken into account in this estimation, could affect the resulting porosity, as well as the choice of Archie’s law constants. Unit II and suspected damaged intervals in Unit III are outside of the curve because of the larger density-derived porosity values caused by hole washouts. Comparison of the resistivity-derived porosity calculated with Archie’s law to the density-derived porosity is also presented in Figure F18. On Figure F18, the density-derived porosity log is also shown for comparison; however, this log has been filtered to remove data from portions of the hole where caliper diameter is >9.5 inches.

Resistivity-derived porosity generally decreases with depth. Bit and ring resistivity–derived porosity show very similar trends except in logging Unit II. In the upper part of logging Unit I, resistivity-derived porosity slowly decreases from 63% at 60 m LSF to 62% at 69 m LSF and is followed by a sharp decrease at its base reaching 57% at 75 m LSF. The boundary between logging Units I and II corresponds to a 7% resistivity-derived porosity increase, reaching 63% at 80 m LSF. Bit resistivity–derived porosity in logging Unit II decreases to an average value of 56% at its base (150 m LSF). Fluctuations of 2%–7% amplitude and 15 m wavelength are superimposed on this decreasing trend. In this logging unit, the difference between ring and bit resistivity–derived porosity is

very large (up to 15%), whereas the difference is small in the other logging units. Logging Unit II is characterized by very high caliper values, suggesting strong washouts. We suggest that the time delay between the two measurements allowed for washout development and resulted in high overestimation of the ring resistivity–derived porosity.

At the transition from logging Unit II to III resistivity-derived porosity sharply decreases from 56% to 47% within a 9 m interval, with a local 44% minimum in between. Resistivity-derived porosity decreases slowly between 47% at 158 m LSF and 41% at 416 m LSF, with a slight 1% increase between 320 and 330 m LSF. Variations with smaller amplitude can also be observed. At 416 m LSF, it begins to increase slowly to reach 43% at 461 m LSF. In this high caliper value interval, density-derived porosity has been filtered out, but the bit resistivity-derived porosity does not seem to be affected by the washout. The lowermost 37 m of the hole shows one sharp 2% amplitude fluctuation over 10 m followed by a second 3% amplitude fluctuation over the remaining 27 m.

Structural geology and geomechanics

Because of the lack of image data and the poor quality of the density and sonic logs, we derived general structural interpretations from the caliper, gamma ray, and resistivity logs. A number of washed out (high caliper) intervals occur in logging Unit III (Table T2; Fig. F8). Because the gamma ray and resistivity logs do not decrease through these intervals they probably represent poorly consolidated argillaceous material or, most likely, fault zones. Three prominent washout zones occur between 416 and 451 m LSF, with several others within tens of meters above and below this interval. This area of the borehole also corresponds to bright tilted reflectors, further strengthening the interpretation of these washout zones as faults.

Log-seismic correlation

Seismic observations and correlation with logging units

Based on the Kumano 3-D seismic volume (Moore et al., 2007), Site C0003 was spudded into the edge of a slope sediment sequence that overlies the thrust sheet of one splay in the megasplay fault system. In detail, this thrust sheet is itself faulted by three additional imaged faults local to the borehole, with additional subseismic-scale faulting being likely.

A prestack depth-migrated (PSDM) dip-parallel image across the site shows a slope sediment sequence with reflectors largely parallel to the seafloor lying unconformably above an older accreted sequence; the contact is a strong positive polarity (same as the seafloor) reflection (Fig. F9). Below this unconformity is a wedge-shaped sequence with an apparently subhorizontal, negative polarity reflection in the center of the wedge and a dipping negative polarity reflection at its base. Two faults that cut through the thrust sheet can be traced to near this wedge-shaped sequence. The tip of the shallower fault cuts toward the seafloor on the northwest side of the sequence; the deeper fault can be traced to near the base of the wedge, but the relationship of this fault to the reflector at the base of the wedge-shaped sequence is unclear (Fig. F9).

The basal reflection from this wedge-shaped sequence displays angular relationships with the underlying reflections. Below it is a low-reflectivity sequence with a thick fault zone at its base. A single prominent reflection within this low-reflectivity sequence lies at ~250 m LSF and could be structural or stratigraphic. The fault zone penetrated near the base of the borehole may be as thick as ~100 m. The fault zone reflectivity is complicated and laterally variable; at the borehole the highest amplitude response is near the base of the fault zone (Fig. F9).

The logging units correlate well with our seismic observations. Logging Unit I lies at the base of the slope sediment section and the logging Unit I/II contact is likely the positive polarity reflection separating the base of the slope sediments and top of the wedge-shaped sequence. The logging Unit II/III contact is the negative polarity reflection at the base of the wedge-shaped sequence. Logging Unit III spans the low-reflectivity sequence including the fault zone to the bottom.

Log-seismic correlation in zones of interest

Logging Unit I/II boundary and the base of slope sediments

The logs through the slope sediments (logging Unit I) differ strongly from logs in the underlying logging Unit II and help to explain the strong reflection that separates these sequences in the seismic data. The density (Fig. F19), gamma ray (Fig. F20), and resistivity (Fig. F21) logs show strong decreases across the boundary, whereas the neutron porosity (Fig. F22) and caliper (Fig. F23) logs show strong increases across the boundary. The sonic log (Fig. F24) included bad values for all of logging Units I and II, as discussed below. The reflection separating the slope sediments from the wedge-shaped sequence is posi-

tive; however, the density log decreases sharply across this boundary. The high caliper values throughout logging Unit II, however, suggest that the density values in Unit II are suspect because of likely washout (Fig. F9), and thus based on the strong positive reflector we anticipate that the density and velocity values within Unit II should be higher than in Unit I.

Logging Unit II and the wedge-shaped sequence

The low gamma ray and resistivity values combined with the high caliper values for logging Unit II are consistent with a sand-rich sequence (Figs. F20, F21, F23). The base of this unit is a strong negative polarity reflection requiring a decrease in velocity and/or density across the boundary (or inherent to the boundary). This observation suggests that the base of logging Unit II consists of higher density material than Unit III. Additionally there is a low-density interval ~3 m below the logging Unit II/III boundary. The combination of these features may explain the negative polarity reflection. The nature of this reflection is addressed through seismogram modeling described below.

Fault region

From 381 to 470 m LSF are a series of washouts (Fig. F9) interpreted based on the ultrasonic caliper (Fig. F23). This zone correlates with reflections that appear related to the fault zone in the thrust sheet. Interestingly, the brightest reflection within the fault-related zone of reflections lies at and just below the lowest of these washouts in a region where the densities are first quite low and then are higher (Fig. F19). Based on the seismic data, the base of the washouts in this zone is a possible location for the active part of the fault zone and the bulk of the washouts is a large damaged zone above it or perhaps a series of faults with overlapping damaged zones. The low gamma ray response across the damaged zone or series of faults suggests that either brecciation associated with faults or a sandy layer may be the cause of the washouts.

Check shot survey

Because the seismicVISION tool and its memory data were lost in the hole, we created a check shot survey using the real-time data transmitted to the surface during drilling. These data, for each depth station, consist of a 300 ms seismic trace window, comprising 15 shot records stacked downhole (Fig. F25). The tool also makes and transmits three first arrival picks and some information about their likely reliability.

The operator was provided a predrilling forecast of the subsurface velocity and one-way traveltimes. During Expedition 314, these predictions were based on the prestack depth migration velocity model at each site. These predictions and the transmitted waveform are used by the operator to determine which pick, if any, is reliable. The operator may choose to accept the first pick, to accept one of the other picks, or to make a new pick from the seismic trace.

Twelve stations were occupied in Hole C0003A. For two of these stations, the waveform data were corrupted during transmission to the surface. Therefore, we used data from 10 stations ranging from 86 to 506 m LSF (Table T5). The first arrival waveforms from these stations are of high quality and we believe that the first arrival picks are nearly as reliable as those obtained using the memory data for other sites (Fig. F25). At seven of the stations, the operator accepted the first tool pick. At the other three stations, the operator made a new pick from the seismic trace. As at the other sites, corrections were made for source time and hydrophone depth. The data were used as for the other sites to obtain long wavelength interval velocities in the hole and to correct the PSDM seismic section at the borehole. The corrected PSDM section was used as the background in Figures F9, F19, F20, F21, F22, F23, and F24.

The check shot times were adjusted using the method of Lizarralde and Swift (1999), assuming a traveltimes picking variance of 1 ms and a smoothing parameter of 0.2. We used a somewhat higher smoothing parameter than at other sites because we do not have the same level of confidence in the picks and because there were fewer data points. The result is a very smooth velocity curve. Although the smoothing parameter could be reduced and slightly more character teased out of the velocity-depth function, we do not think that it would be statistically justified.

We plotted the smoothed check shot interval velocities with the real-time sonic log velocities (Fig. F26). Unlike the sonic velocity data from other sites, these data were picked by the tool downhole. Only the arrival time picks were sent to the surface; no waveforms were transmitted or otherwise available for surface analysis. For the other sites, extensive reprocessing and manual interpretation of the sonic waveforms were performed. Therefore, we do not expect the real-time sonic log velocities to be reliable. The data show that above ~151 m LSF in logging Units I and II, the sonic log velocities are scattered and much faster than the check shot velocities. We suggest that the sonic velocities in this region should be ignored. Below ~151 m LSF in logging Unit III, the

real-time sonic log velocities are also scattered but the check shot velocity function generally corresponds to their upper bound. Although there seems to be some relationship between the deeper real-time sonic log velocities and the check shot data, we do not think that the sonic velocities can be considered reliable.

Without the longer seismic records recorded in the seismicVISION tool, it is not possible to calculate a vertical seismic profile.

Seismogram modeling

Good quality *P*-wave velocity data from sonicVISION tool are not available because memory data to be reprocessed were not retrieved at this site. Furthermore, the real-time density data in logging Unit II do not reconcile with the polarity of the seismic reflection data as discussed above. These problems meant that we could not generate a meaningful synthetic seismogram from logging data at this site. We therefore tried to calculate seismograms to fit with the observation of the seismic profile. The interpolated smoothed interval velocities from check shot data were used as *P*-wave velocities (Fig. F27B) after slight modification within the water column and depths shallower than ~43 m LSF. The real-time density data were edited as described below. First, we removed the singular density value of 1.82 g/cm³ at 44 m LSF, which is significantly larger than the average density value of ~1.5 g/cm³ at this depth. Next, the real-time density data were edited to remove densities associated with large ADIA values. We chose a cutoff value of 10.5 inches for this purpose after testing values of 9.5, 10.0, and 10.5 inches. To correlate the calculated seismogram with the seismic section we modeled the density data at the logging Unit I/II and II/III boundaries. We assumed that density data increase from 1.62 to 1.72 g/cm³ at 71 m LSF, which is ~5 m shallower than the Unit I/II boundary, and decrease from 2.10 to 1.97 g/cm³ at the Unit II/III boundary. The density data within Unit II were not modeled and thus were interpolated linearly. The modeled density curve (Fig. F27C) was used for seismogram modeling. We used a zero-phase 256 ms wavelet retrieved from cross-line prestack time-migrated (PSTM) section at the vicinity of the site. The modeled seismogram is shown in Figure F27D. Note that the modeled seismogram senses only the density data because *P*-wave velocity is smoothly varying. The modeled seismogram matches with the major features of the seismic section (Fig. F27G–F27I). Both a positive reflector at the boundary between logging Units I and II and a negative amplitude reflection at the base of logging Unit II are reproduced in the modeled seismogram. The depth difference of these reflectors between the

depth-converted PSTM section and the modeled seismogram was <5 m.

The modeling result supports the possibility that density values increase at the Unit I/II boundary and decrease at the Unit II/III boundary. The reflective zone at ~500 m LSF in the seismic section can be correlated with the large-amplitude wave packets in the modeled seismogram; however, we cannot exactly fit the modeled seismogram to the seismic section. This is probably caused by the low quality of real-time logging data. Note that because we assume the density and velocity data are smoothly increasing in logging Unit II, we lose any obvious reflection events within this unit.

Discussion and synthesis

Because our data from Site C0003 is limited to the real-time data transmitted uphole during drilling from 0 to 525 m LSF, we have relatively little information on which to draw conclusions at this site. However, we can draw some inferences on the composition of the thrust sheet in the drilled interval. Consistent with the other midslope sites, the lithology is of apparently relatively coarse silt-sand and hemipelagic mud in the shallowest portion, interpreted as slope sediments based on seismic interpretation (logging Units I and possibly II). These coarser sediments are underlain by more clay rich, generally homogeneous muddy deposits of logging Unit III, interrupted by prominent zones of washouts interpreted as brecciated intervals, indicating likely faults. The seismic reflection imaging shows that this site was drilled into a series of at least three individual thrust sheets within the hanging wall of the megasplay fault system (Fig. F28). The seismic character with numerous landward-dipping reflectors indicates that the hanging wall block (or thrust sheet) contains numerous thrusts below the resolution of seismic reflection data. In fact, PSDM versions of the data that became available just as we went to sea made this fabric clear, though it was not visible in the time-processed seismic volume. Therefore, the major washout zones at ~240 and 420–450 m LSF are likely to be strongly brecciated damage zones from subsidiary thrusts.

The seismic interpretation is consistent with substantial uplift of the thrust sheet bringing older accretionary prism rocks to within 500 m of the seafloor. Log density data show relatively constant and high values for this depth, suggesting that anomalously well-indurated rocks make up the thrust sheet. When the broken section of drill pipe was recovered to the rig floor after loss of the LWD string, it was plugged with cuttings and numerous large blocks (as large as 5–8 cm in diameter) of cavings that had come from an unknown position in the hole. This material had a nannofossil age of late Miocene (5.5–7.2 Ma), bulk density of 2.1 g/cm³ (implying a porosity of ~35%), and *P*-wave velocity of ~2.1 km/s. It is remarkably well lithified for material from <530 mbsf, which is also consistent with the thrust sheet rocks having been uplifted from substantially greater depth within the accretionary complex.

In summary, the portion of the thrust sheet penetrated at Site C0003 was largely homogeneous material, most likely sandy to clayey hemipelagic muds, and clearly heavily deformed by multiple faults and associated brittle fractures. Some evidence suggests that this thrust sheet has been transported a substantial distance vertically by thrusting, bringing older, denser rocks to shallow depths.

References

- Lizarralde, D., and Swift, S., 1999. Smooth inversion of VSP traveltime data. *Geophysics*, 64(3):659–661. doi:10.1190/1.1444574
- Mikada, H., Becker, K., Moore, J.C., Klaus, A., et al., 2002. *Proc. ODP, Init. Repts.*, 196: College Station, TX (Ocean Drilling Program). doi:10.2973/odp.proc.ir.196.2002
- Moore, G.F., Bangs, N.L., Taira, A., Kuramoto, S., Pangborn, E., and Tobin, H.J., 2007. Three-dimensional splay fault geometry and implications for tsunami generation. *Science*, 318(5853):1128–1131. doi:10.1126/science.1147195
- Moore, G.F., Taira, A., Klaus, A., et al., 2001. *Proc. ODP, Init. Repts.*, 190: College Station, TX (Ocean Drilling Program). doi:10.2973/odp.proc.ir.190.2001

Publication: 5 March 2009
MS 314315316-115



Figure F1. Summary log diagram, Site C0003. Because of the loss of logging-while-drilling bottom-hole assembly at 525 m LWD depth below seafloor (LSF), only real-time data is available. VE = vertical exaggeration.

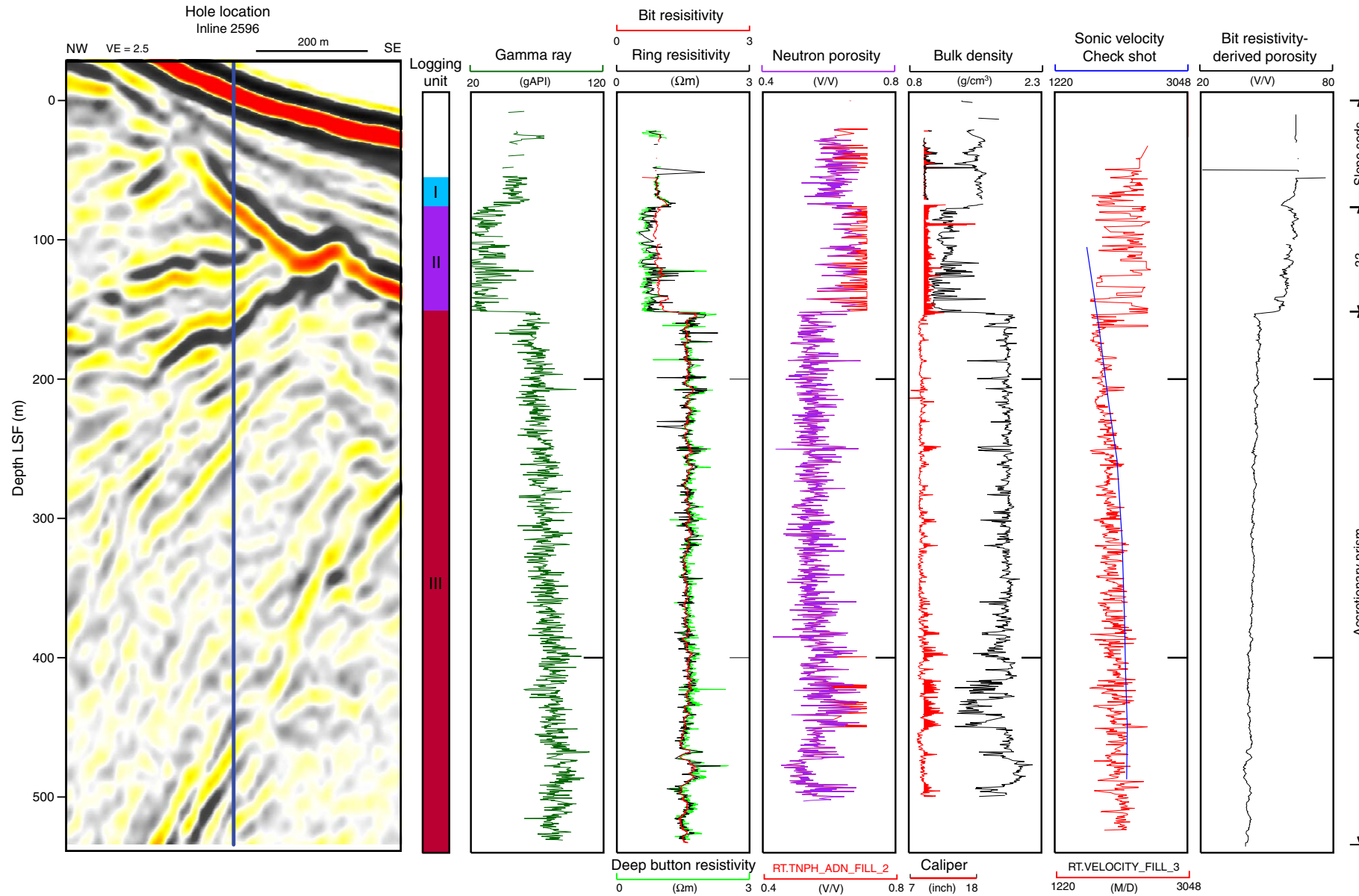


Figure F2. Three-dimensional seismic profile crossing Site C0003 (Moore et al., 2007). A. Inline 2596. B. Cross-line 5389. VE = vertical exaggeration.

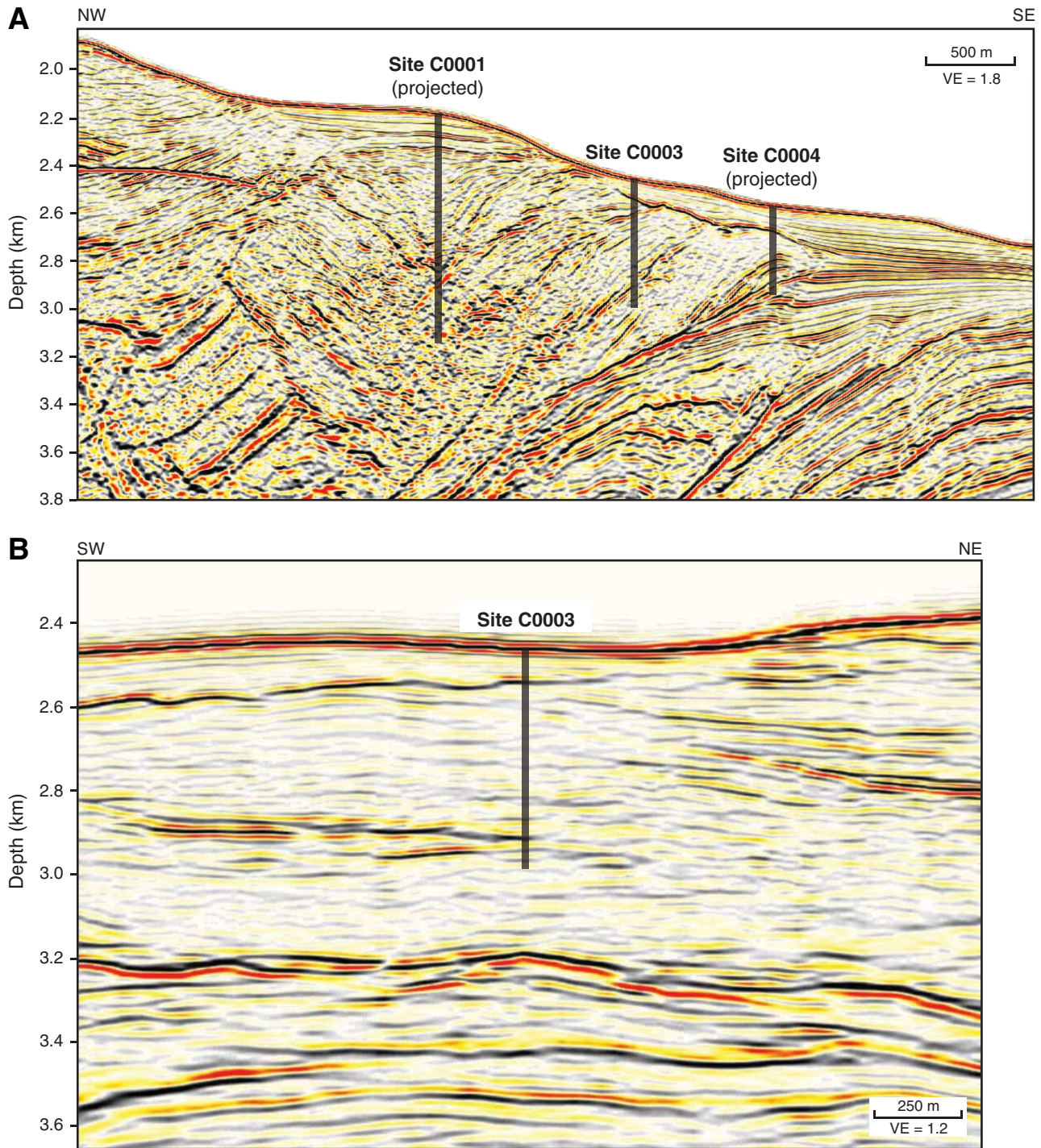


Figure F3. Diagram of final hole condition at time of plugging and abandonment. OD = outer diameter, DRF = drillers depth below rig floor, DSF = drillers depth below seafloor, LWD = logging while drilling, ADN = Azimuth Density Neutron tool.

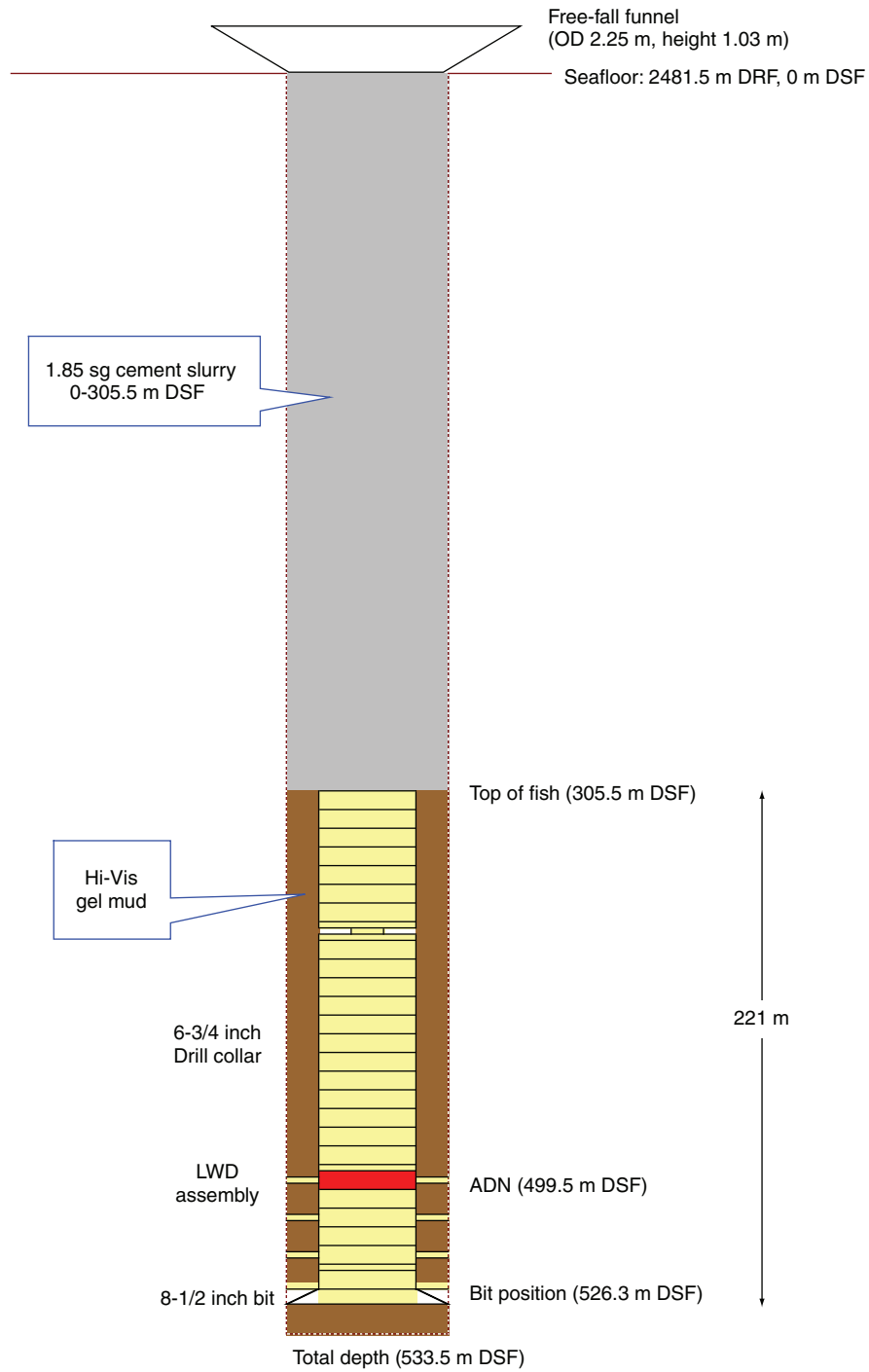


Figure F4. Drilling parameters and gamma ray log vs. time for MWD-APWD operations in Hole C0003A. ATMP_MWD = annular temperature from the real-time APWD tool, GR_RAB_RT = gamma ray resistivity-at-the-bit (real time), ECD = equivalent circulating density, APRS = average annular pressure, TRPM = MWD turbine rotation speed, TRPM_RT = TRMP (real time), CRPM = collar rotation, SWOB = surface weight on bit, HKLD = hook load, SPPA = standpipe pressure, ROP = rate of penetration, ROP_5ft = 5 feet averaged ROP, LSF = LWD depth below seafloor, DRF = drillers depth below rig floor.

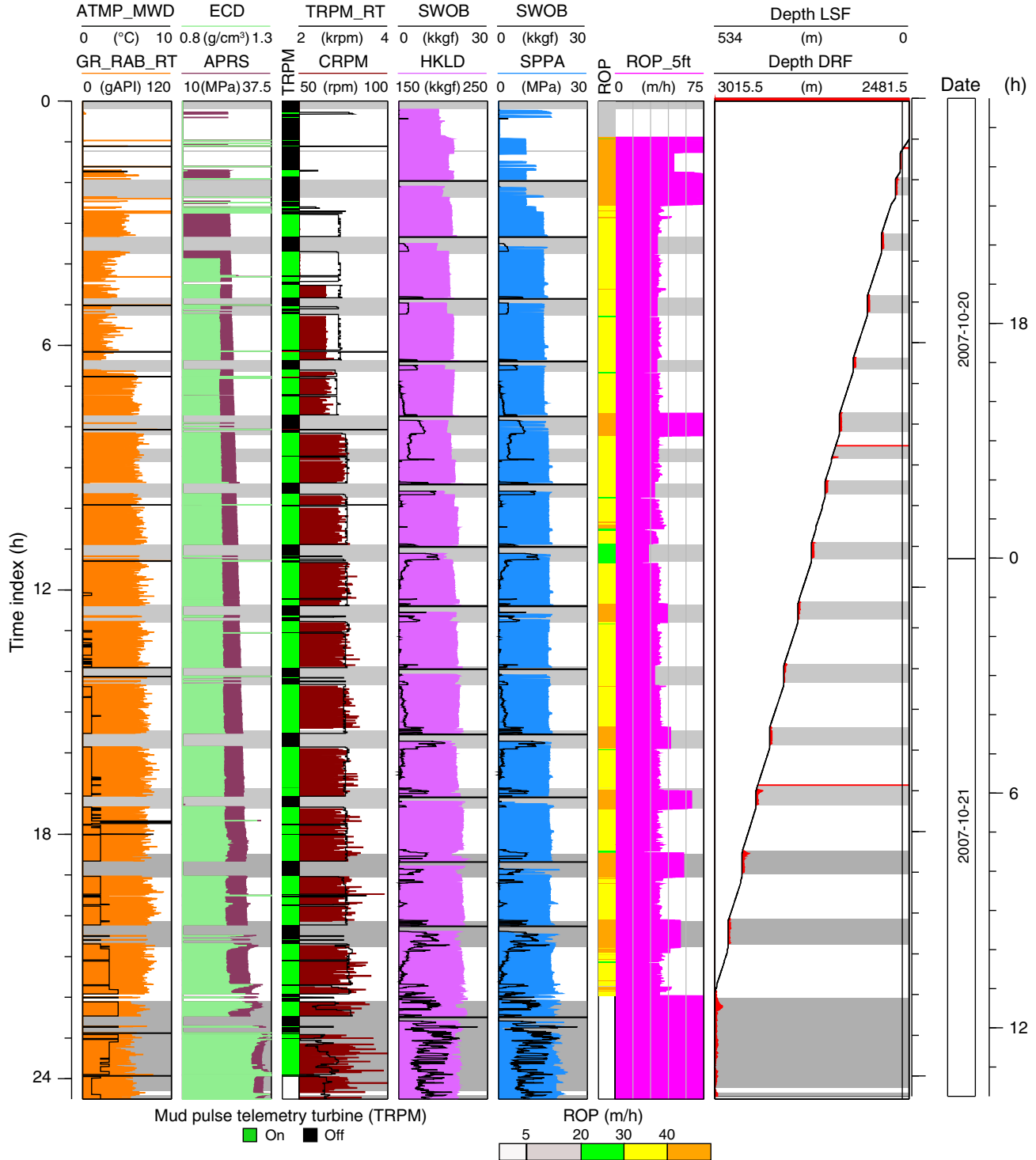


Figure F5. Real-time control logs of Hole C0003A. Fluid pulse telemetry began transmitting real-time data from ~50 m LSF (bit depth). Yellow = no reading of the geoVISION tool, orange = no reading of the adnVISION tool. LSF = LWD depth below seafloor, SWOB = surface weight on bit, ROP = rate of penetration, SPPA = standpipe pressure, HKLD = hook load, CRPM = collar (bit) rotation speed, ADIA= ultrasonic caliper from the adnVISION tool, HDEVI = hole deviation, ECAL_RAB = resistivity-derived caliper from the geoVISION resistivity (GVR) tool, APRS = average annular pressure, ECD = equivalent circulating density, ATMP_MWD = average annular temperature, SHK_R = radial shocks and SHK_T = tangential shocks on the geoVISION tool, STICK = stick slip indicator, SHKPK = shock peak level, GR = gamma ray log from the GVR tool, RES_BD = deep button resistivity, RES_RING = ring resistivity, RHOB_DH = bulk formation density computed downhole, DRHO_DH = bulk density correction also computed downhole, DTCO = transit time of compressional wave automatically picked downhole, V_p = velocity of compressional wave derived from DTCO. (Figure shown on next page.)



Figure F5 (continued). (Caption shown on previous page.)

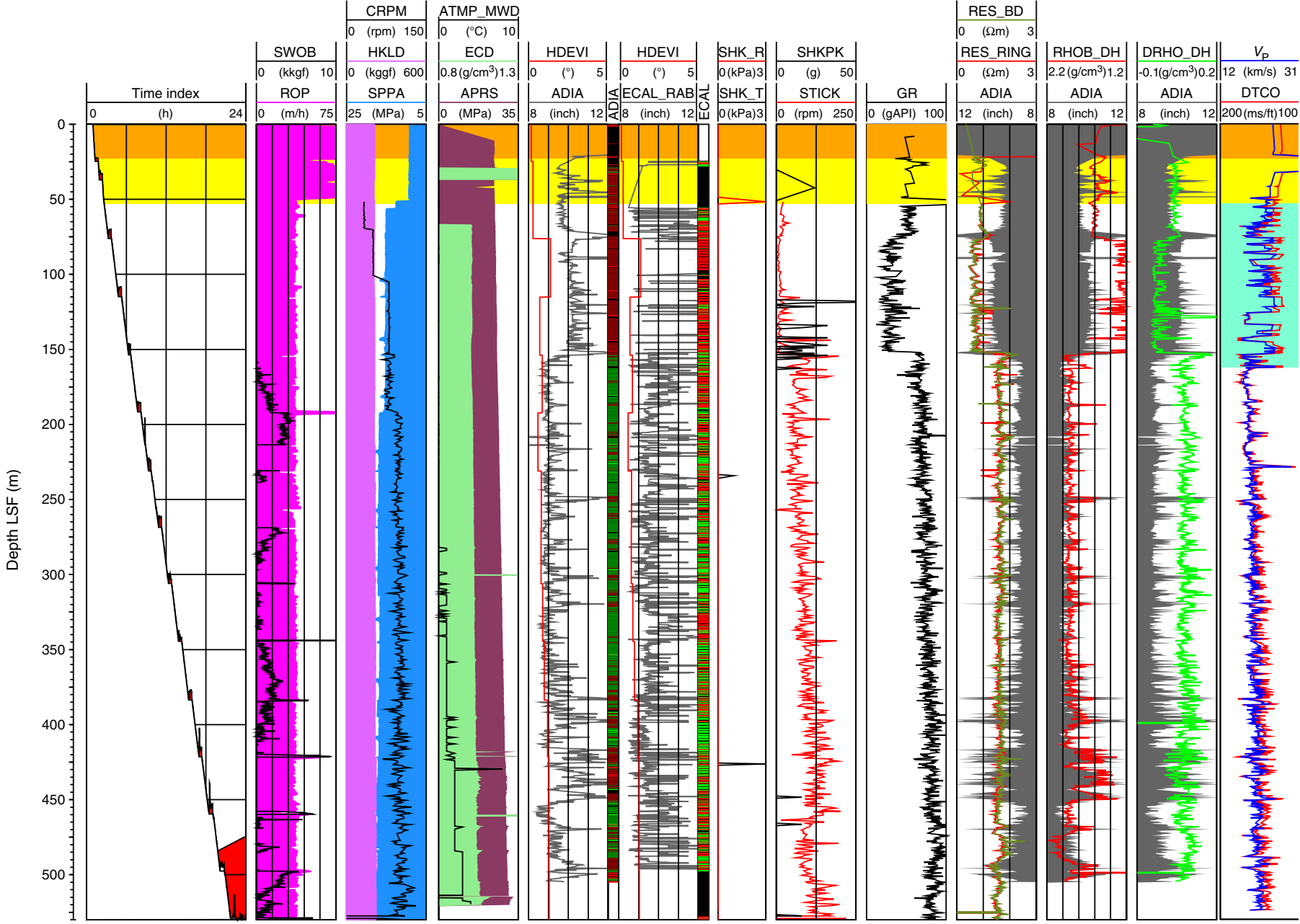


Figure F6. Plot of time vs. depth in Hole C0003A. LSF = LWD depth below seafloor.

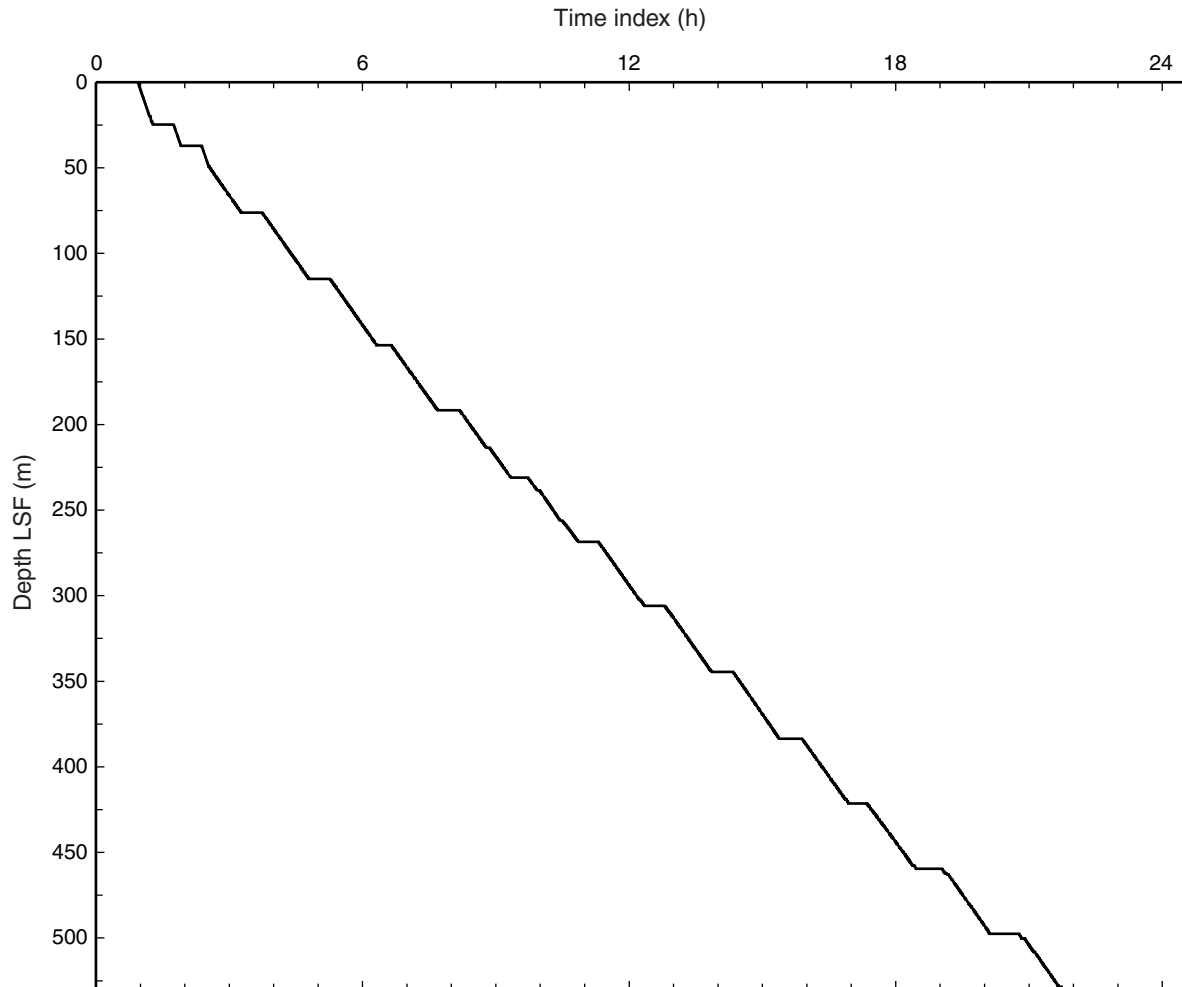




Figure F7. Statistical variation of logging Units I-III.

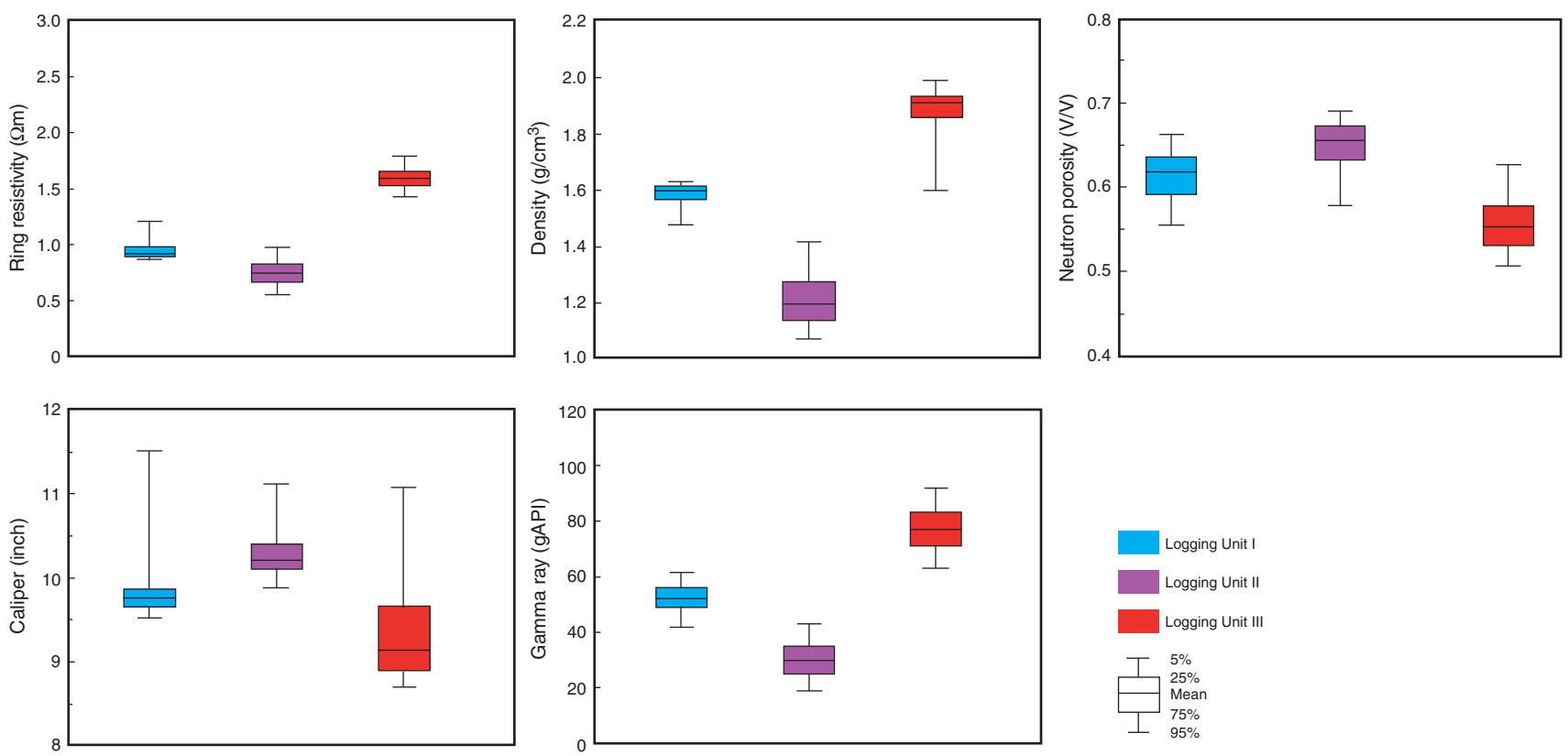


Figure F8. Interpreted washed out zones within logging Unit III. Zones were picked primarily based on abrupt increases in real-time caliper values, often associated with abrupt density lows. Washouts are not correlated with local lows in the gamma ray log, implying a cause other than increased sand content. Variability of gamma ray and resistivity logs within most of these zones may indicate a deformed or fractured zone. LSF = LWD depth below seafloor.

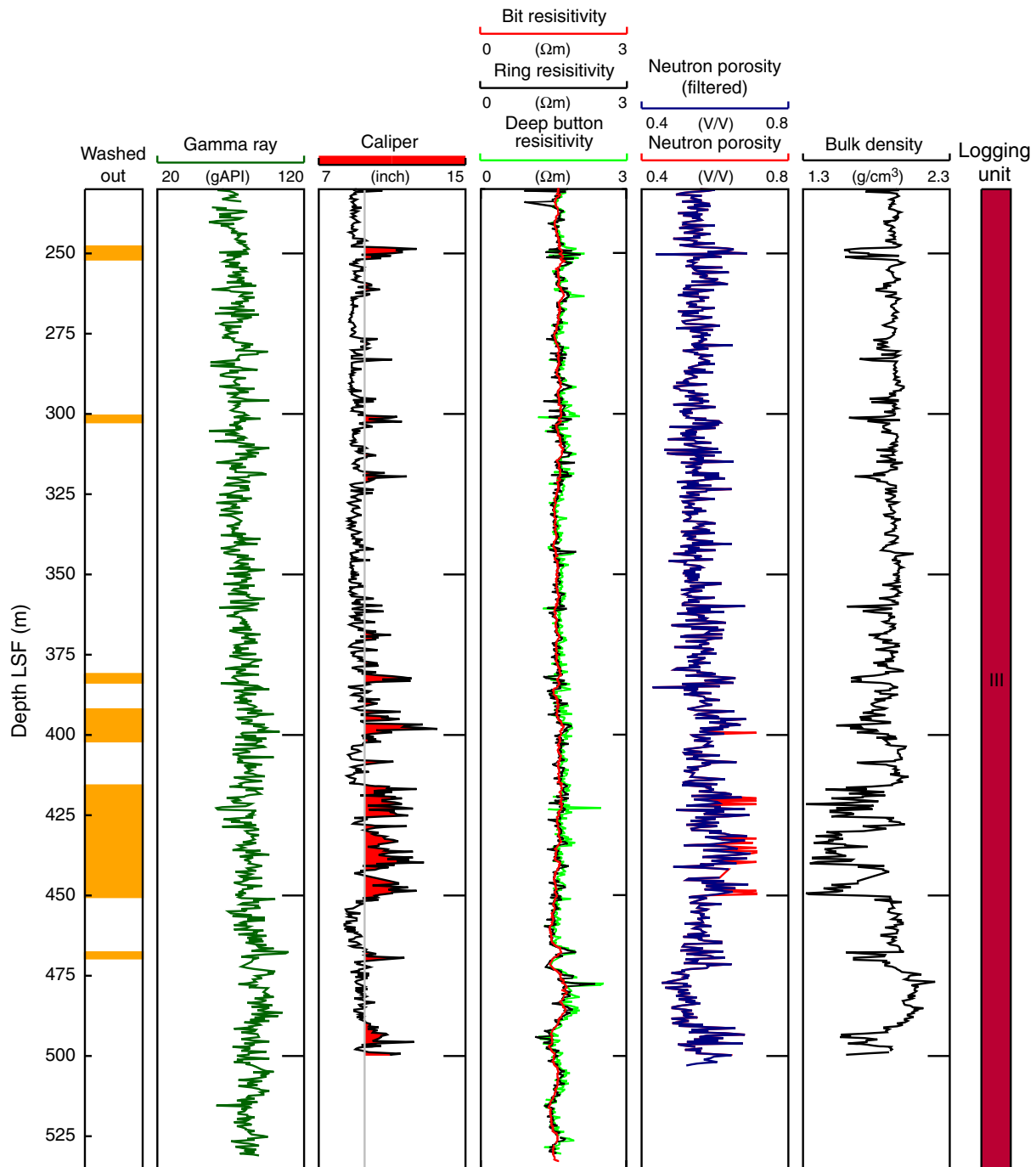


Figure F9. Logging Units I–III and potential washouts superimposed on check shot–corrected prestack depth-migrated seismic profile through Hole C0003A. Three faults interpreted based on crosscutting character and reflectivity. Note the strong positive polarity reflection (red) separating the slope sediments from a wedge-shaped sequence at Unit II and the strong negative polarity reflection at the base of the wedge-shaped sequence. On this figure and the similar figures the borehole is located at distance = 0 with the log or units displayed to the side. LSF = LWD depth below seafloor, VE = vertical exaggeration.

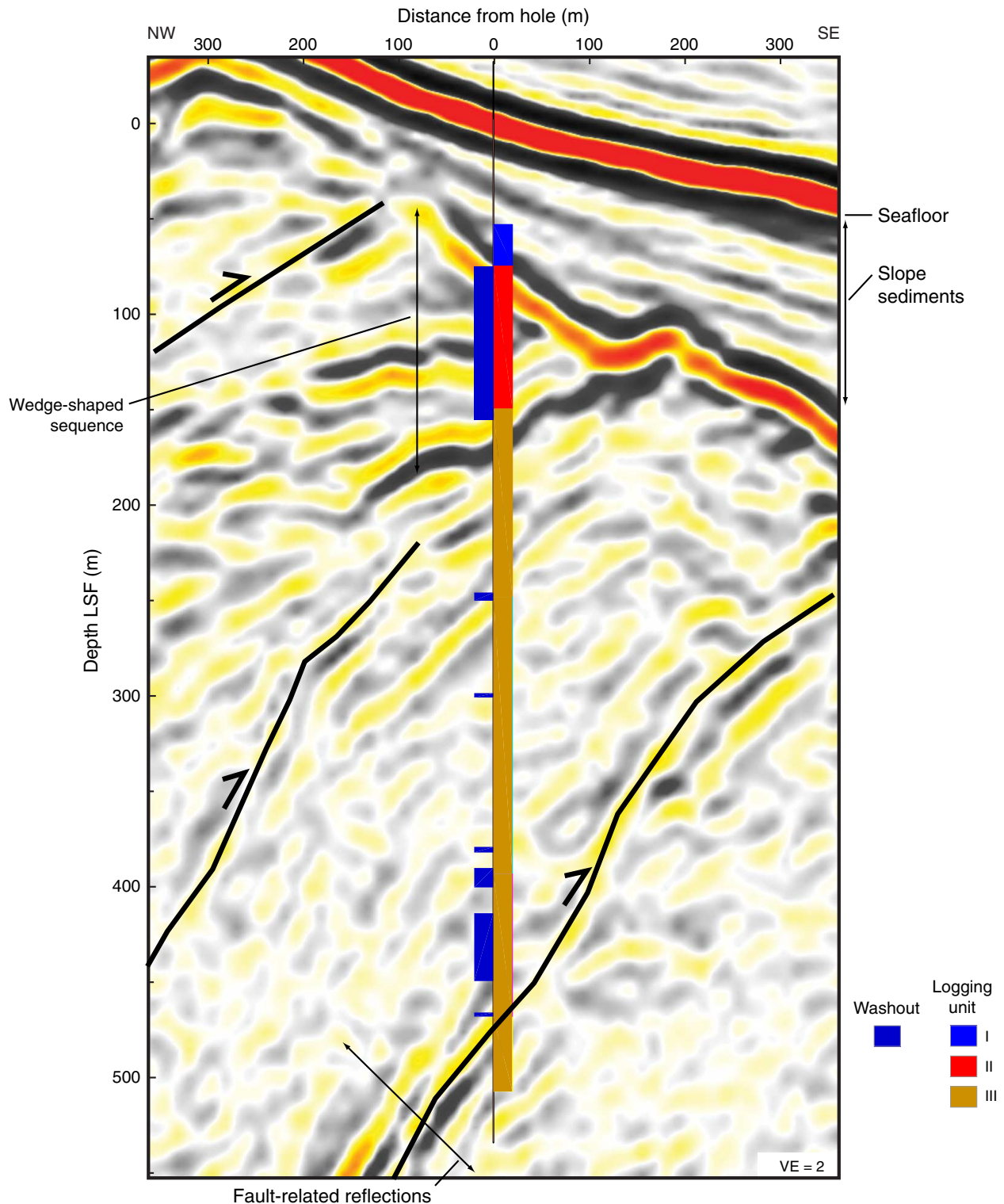


Figure F10. Gamma ray comparison at Sites C0001, C0002, C0003, and 808.

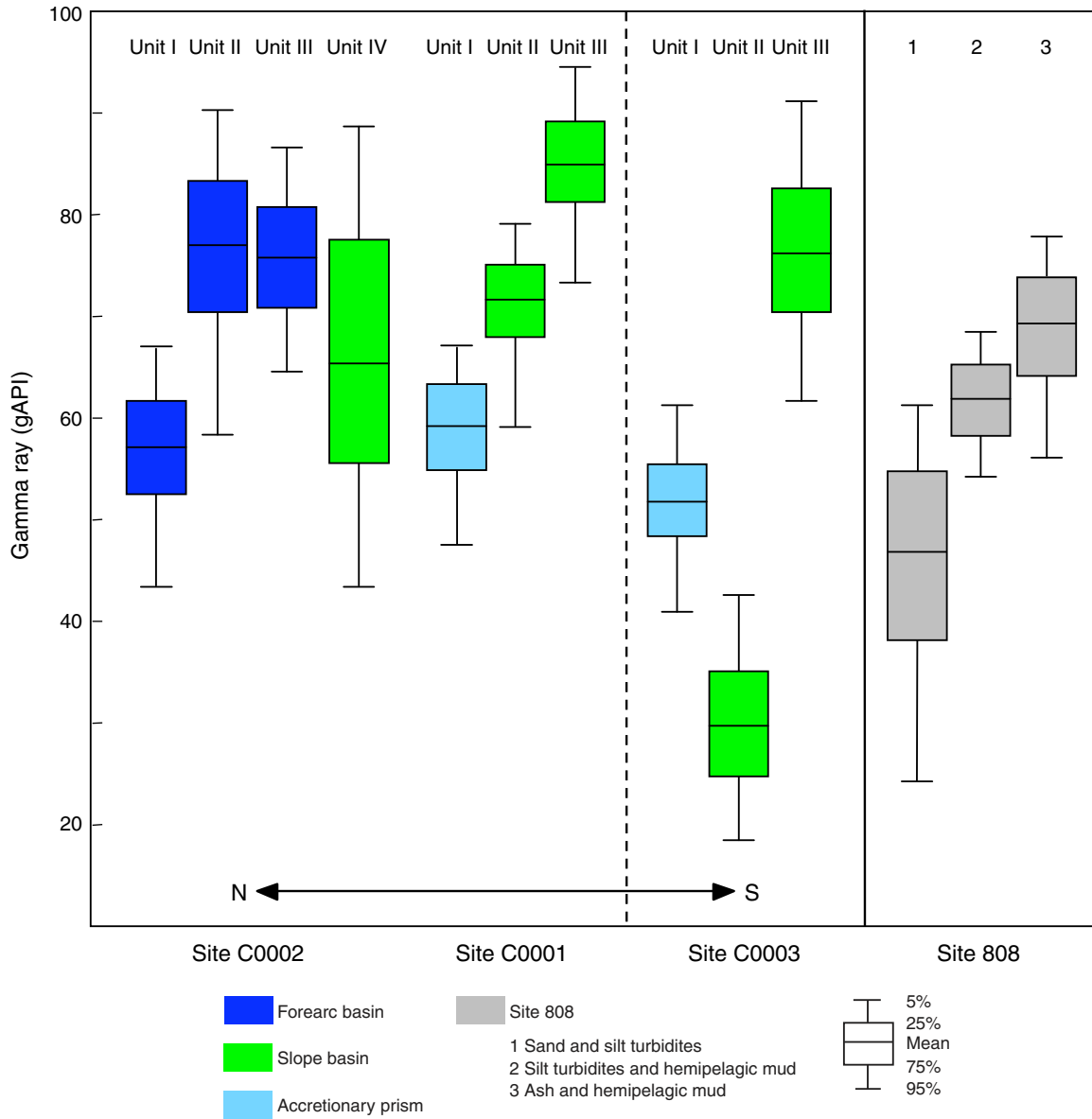


Figure F11. Real-time bulk density data (RHOB) profile from Hole C0003A and ADIA caliper data. Red zones on caliper log = caliper values >9.5 inches interpreted as washout zones, gray zones = potential deformation-related washed out zones as defined in “**Log characterization and lithologic interpretation.**” LSF = LWD depth below seafloor.

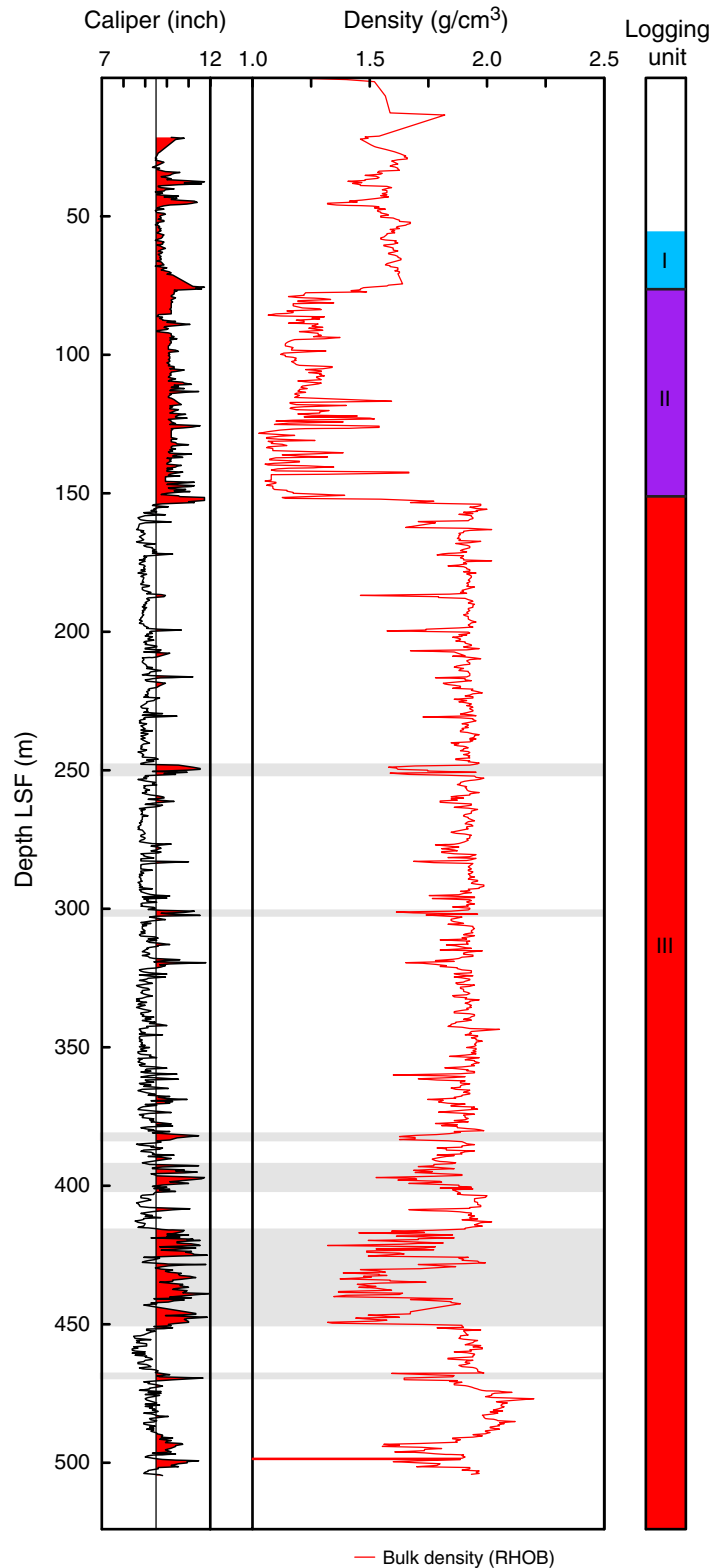


Figure F12. Neutron and density-derived porosity profile from Hole C0003A shown with ECAL and ADIA calipers. Red zones on caliper log = caliper values >9.5 inches interpreted as washout zones, gray zones = potential deformation-related washed out zones as defined in “Log characterization and lithologic interpretation.” LSF = LWD depth below seafloor.

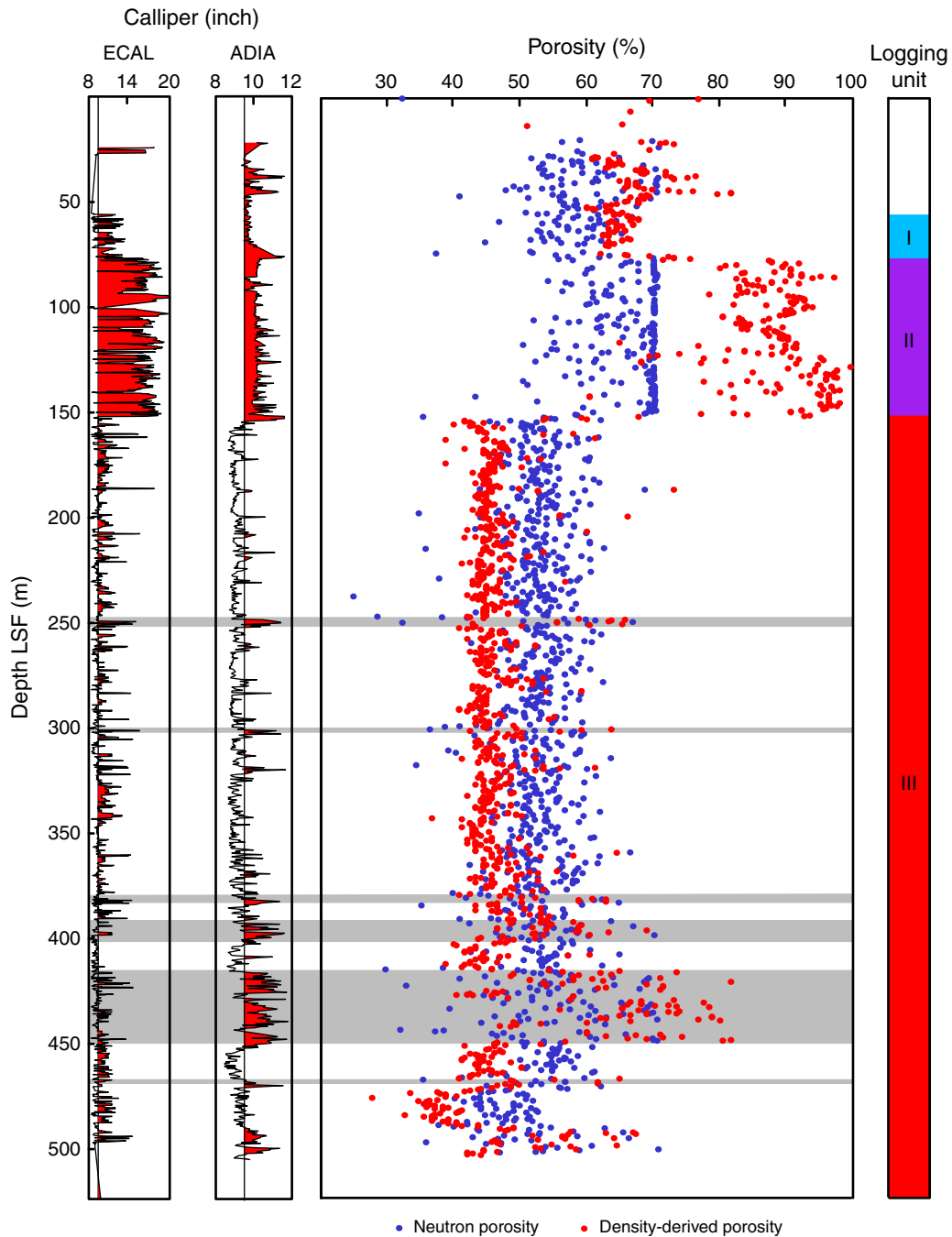


Figure F13. Neutron vs. density-derived porosity. Solid line = unit slope passing through the origin.

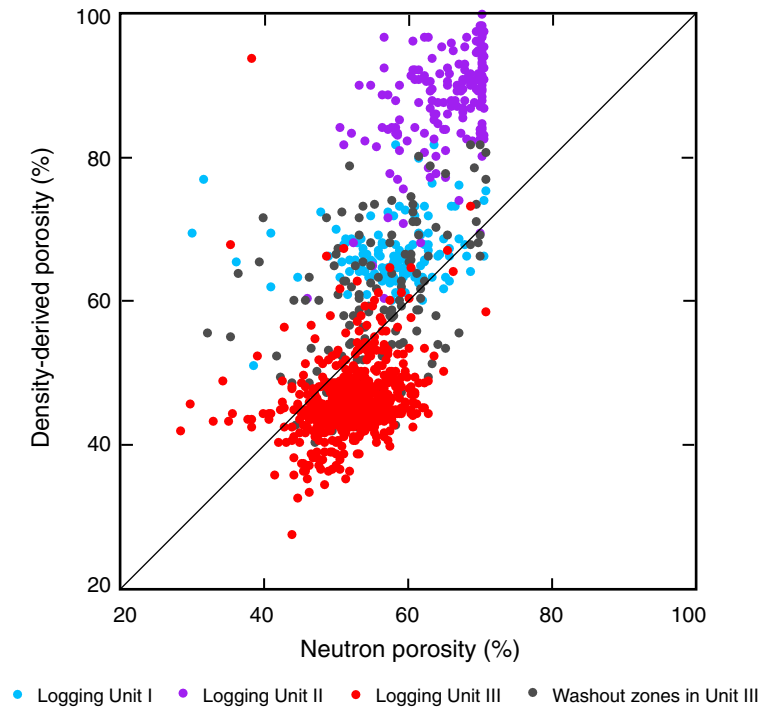


Figure F14. Real-time thermal neutron porosity ultrasonic caliper (corrected) (TNUC) data profile from Hole C0003A and smoothed porosity data using a 4.5 m running average and ADIA caliper data. Red zones on caliper log = caliper values >9.5 inches interpreted as washout zones, gray shading = potential deformation-related washed out zones as defined in “**Log characterization and lithologic interpretation.**” LSF = LWD depth below seafloor.

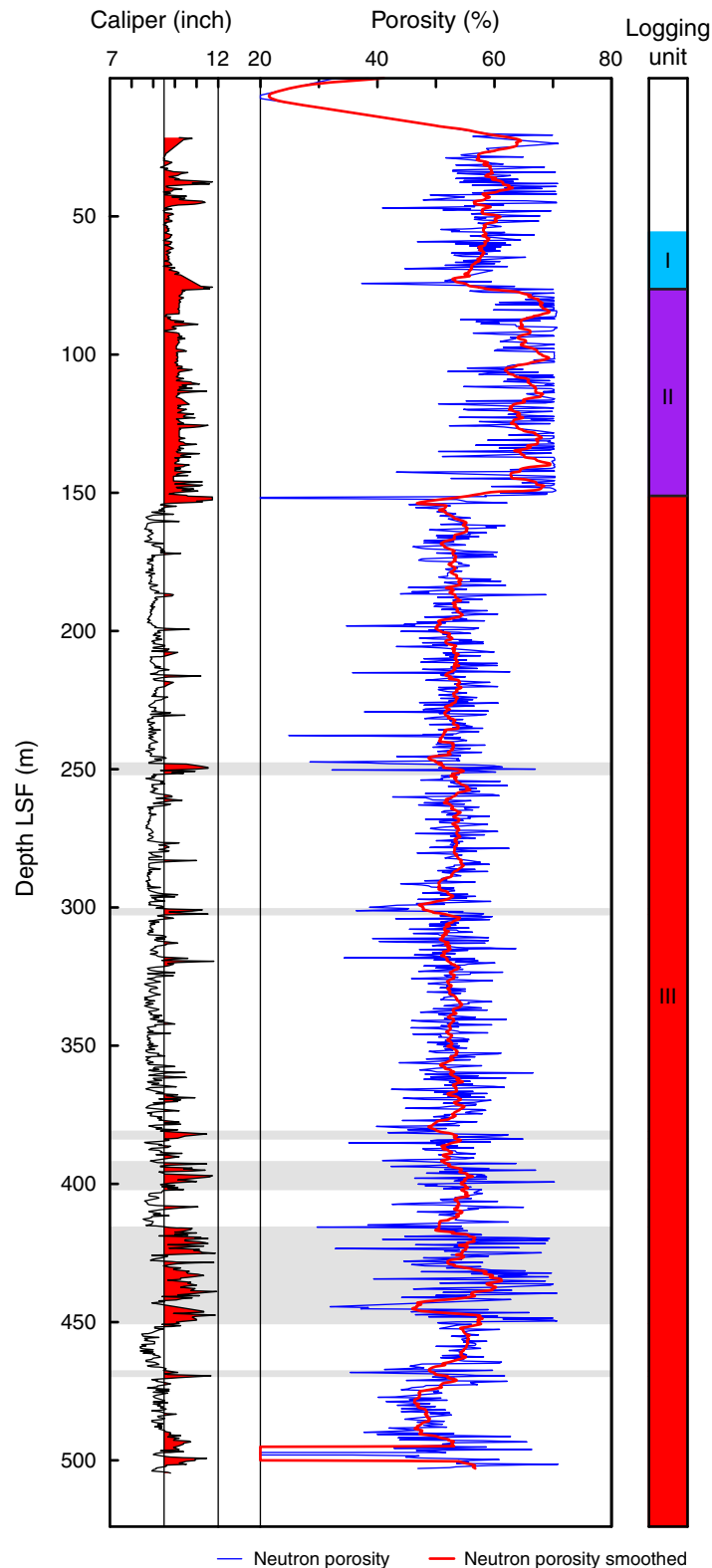


Figure F15. Ring and bit resistivity log and deep button resistivity log shown with ECAL and ADIA calipers. Red zones on caliper log = caliper values >9.5 inches interpreted as washout zones, gray zones = potential deformation-related washed out zones as defined in “**Log characterization and lithologic interpretation.**” LSF = LWD depth below seafloor.

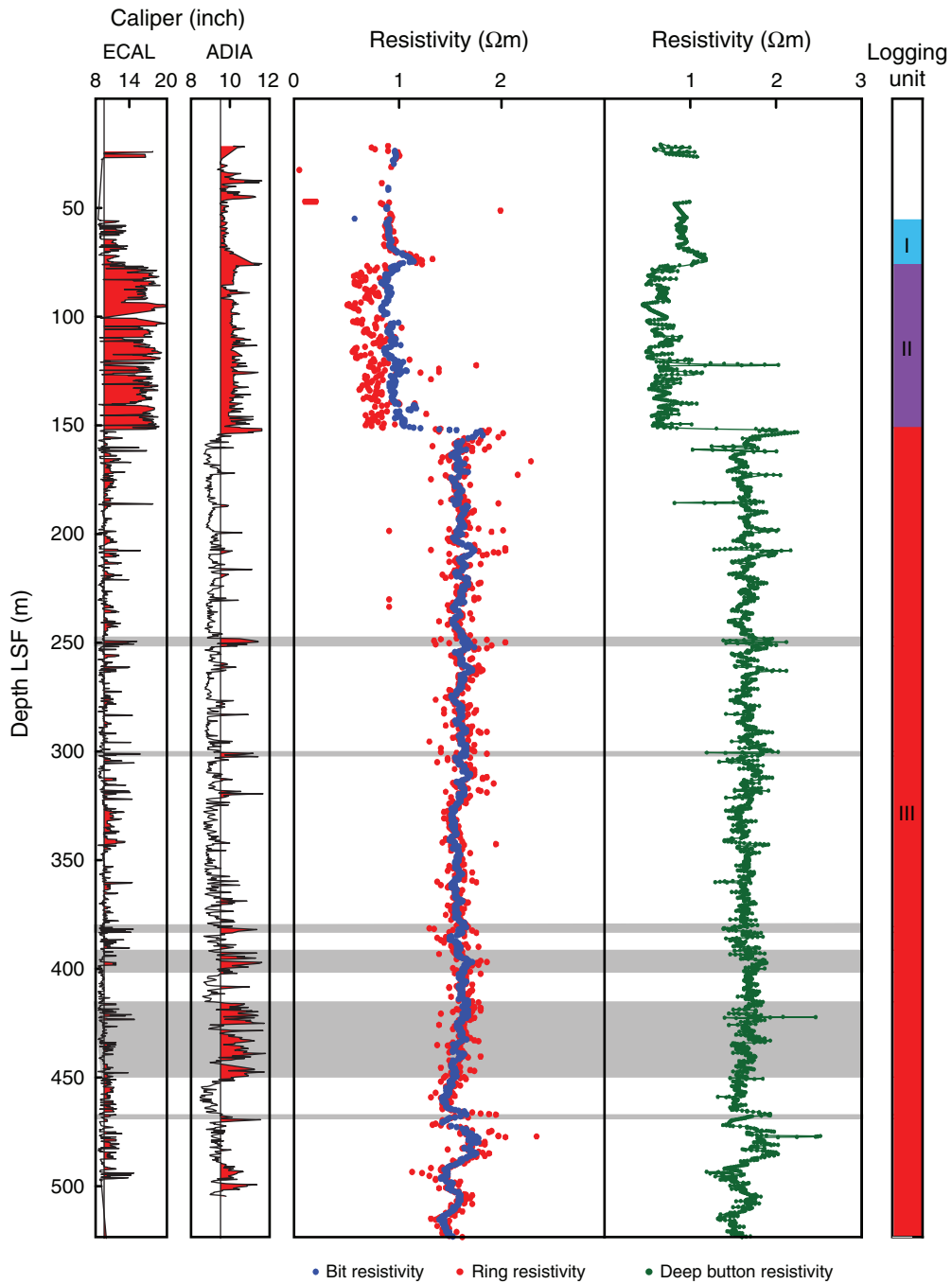


Figure F16. Plot of bit vs. ring resistivity. Solid line = unit slope passing through the origin.

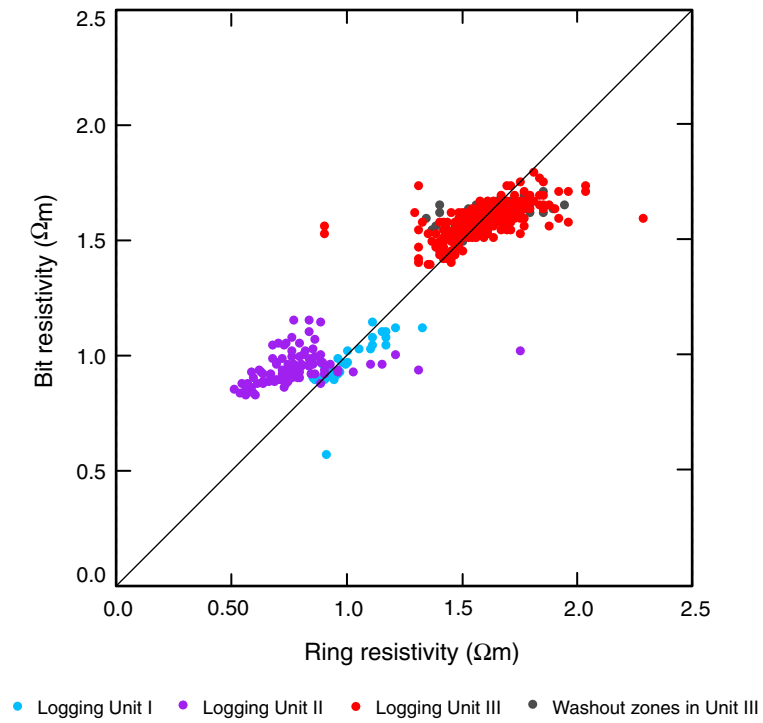


Figure F17. Plots of ring and bit formation factor (FF) vs. bulk density (RHOB)-derived porosity. Solid curves correspond to the plot of the best-fit Archie's law formation factor ($FF = 1/\phi^{-2.4}$).

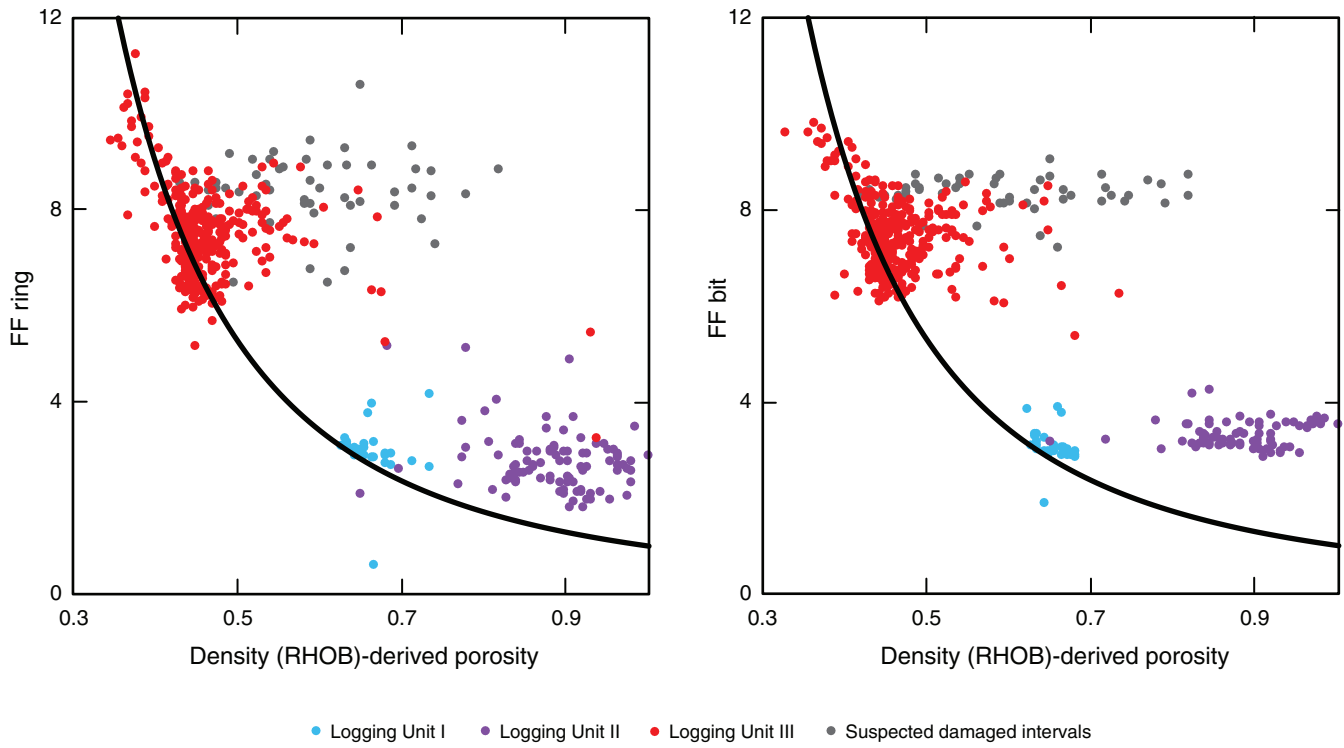


Figure F18. Azimuthal Density Neutron (ADN) caliper values (red = >9.5 inches) and bit and ring resistivity-derived porosity (Archie’s law parameters $a = 1$ and $m = 2.4$) compared with bulk density (RHOB)–derived porosity. Red zones on caliper log = caliper values >9.5 inches interpreted as washout zones, gray shading = potential deformation-related washed out zones as defined in “**Log characterization and lithologic interpretation.**” LSF = LWD depth below seafloor.

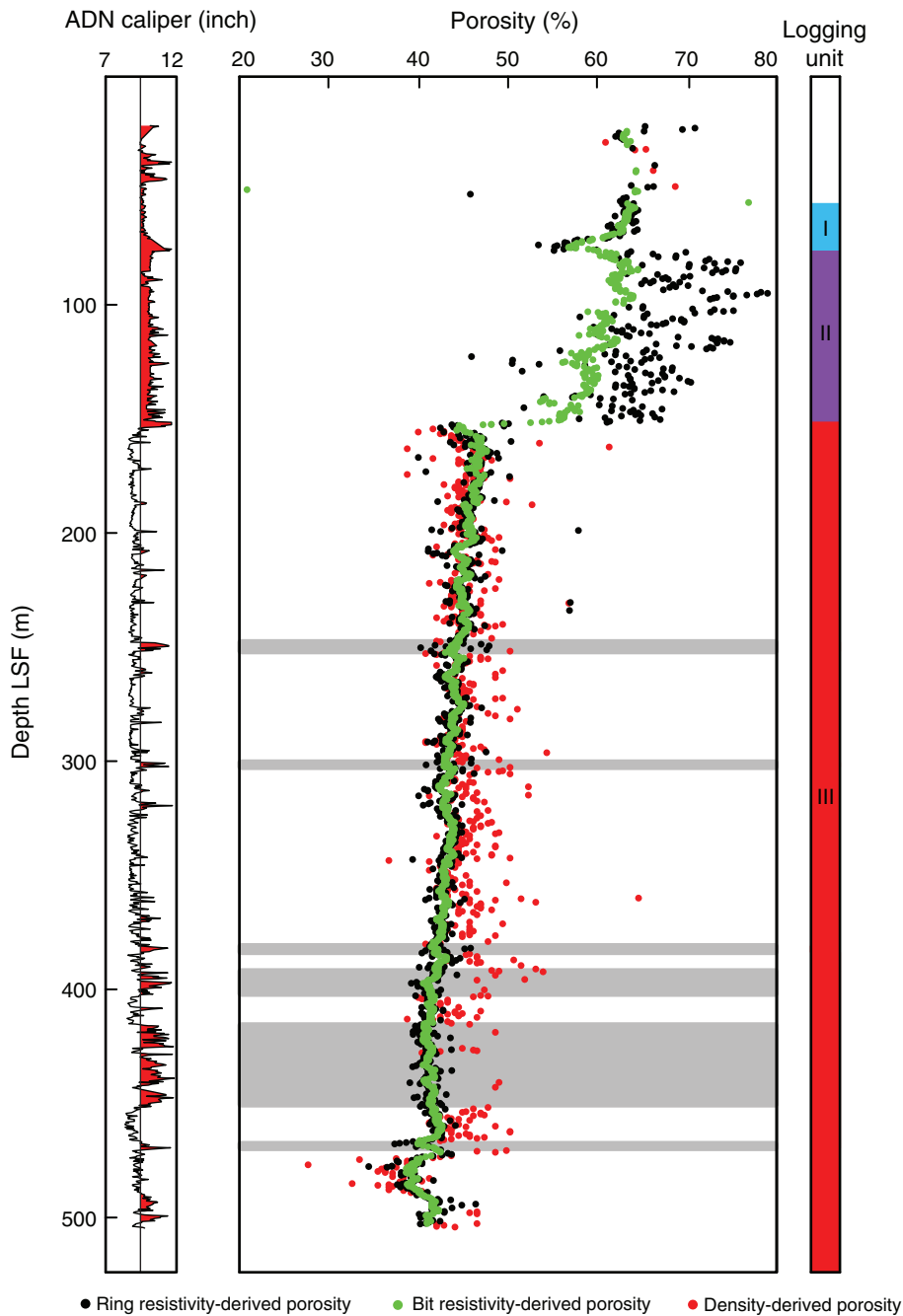


Figure F19. Real-time density log superimposed on check shot–corrected prestack depth-migrated seismic profile through Hole C0003A. See “Data and log quality” for important discussion of the quality of this density data, however. LSF = LWD depth below seafloor, VE = vertical exaggeration.

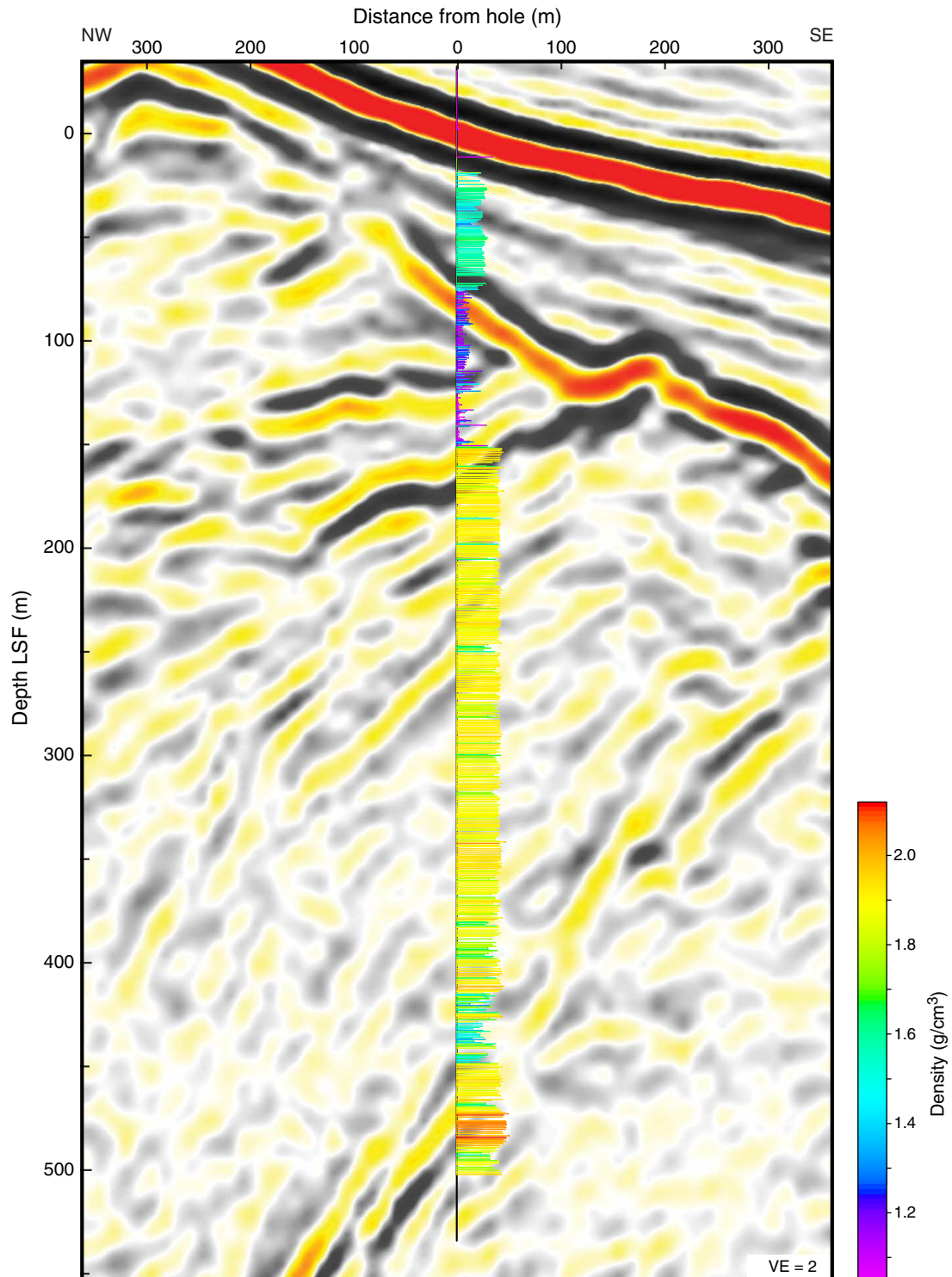


Figure F20. Real-time gamma ray log superimposed on check shot-corrected prestack depth-migrated seismic profile through Hole C0003A. Note the extremely low values for the wedge-shaped sequence at logging Unit II, suggestive of sands. LSF = LWD depth below seafloor, VE = vertical exaggeration.

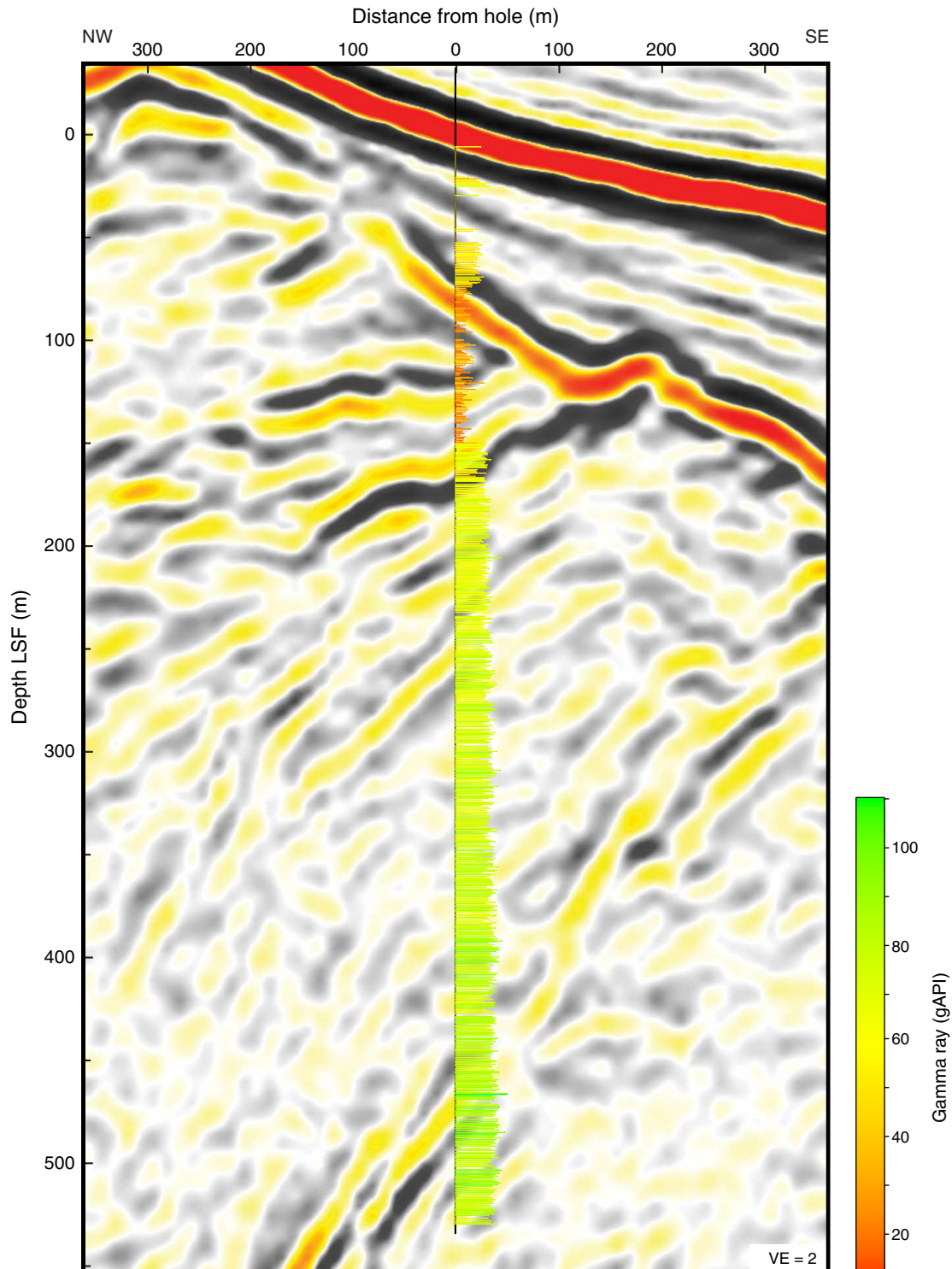


Figure F21. Real-time ring (left) and bit (right) resistivity logs superimposed on check shot–corrected prestack depth-migrated seismic profile through Hole C0003A. Color scale is logarithmic. LSF = LWD depth below seafloor, VE = vertical exaggeration.

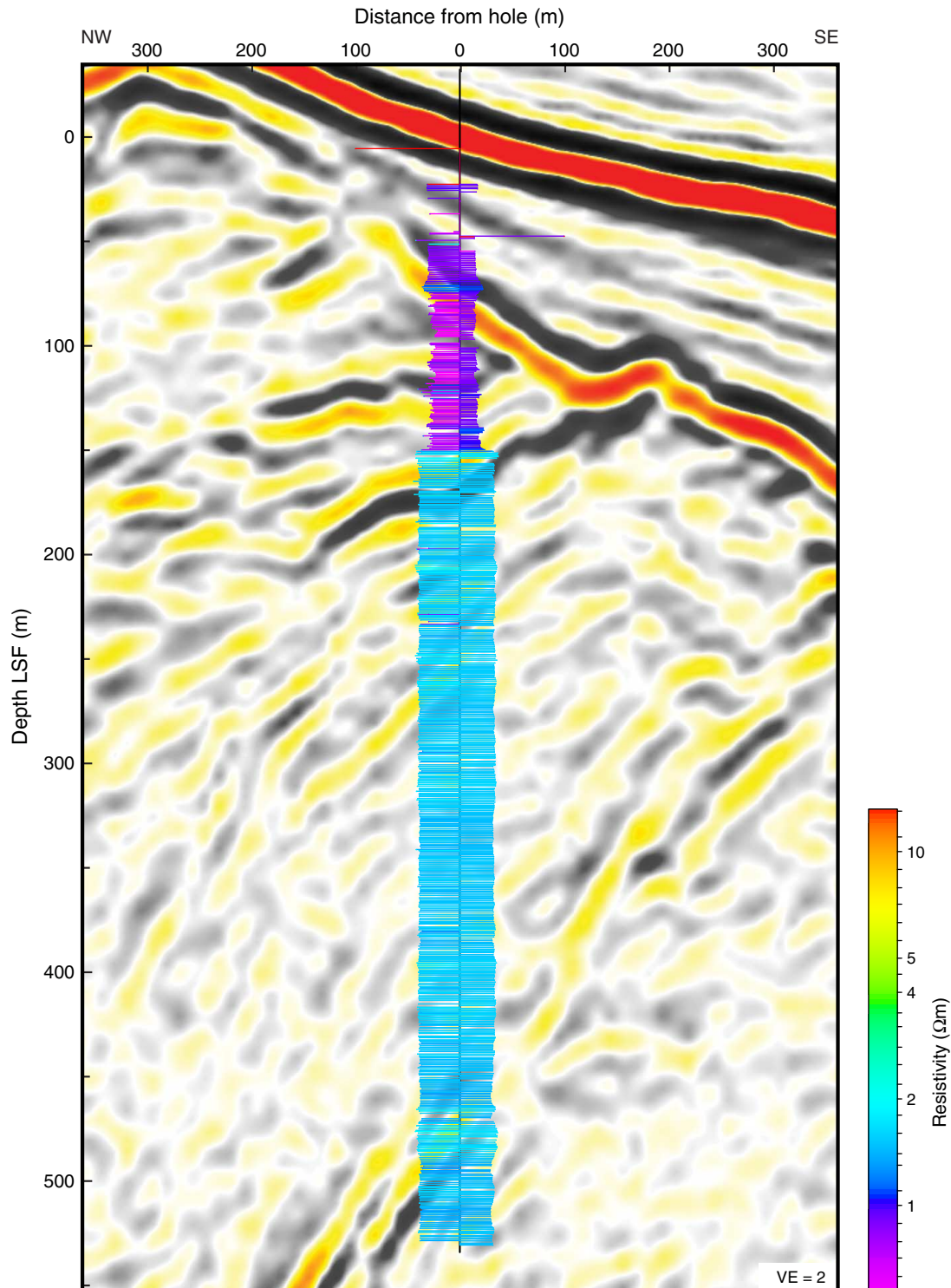


Figure F22. Real-time neutron porosity log superimposed on check shot–corrected prestack depth-migrated seismic profile through Hole C0003A. LSF = LWD depth below seafloor, VE = vertical exaggeration.

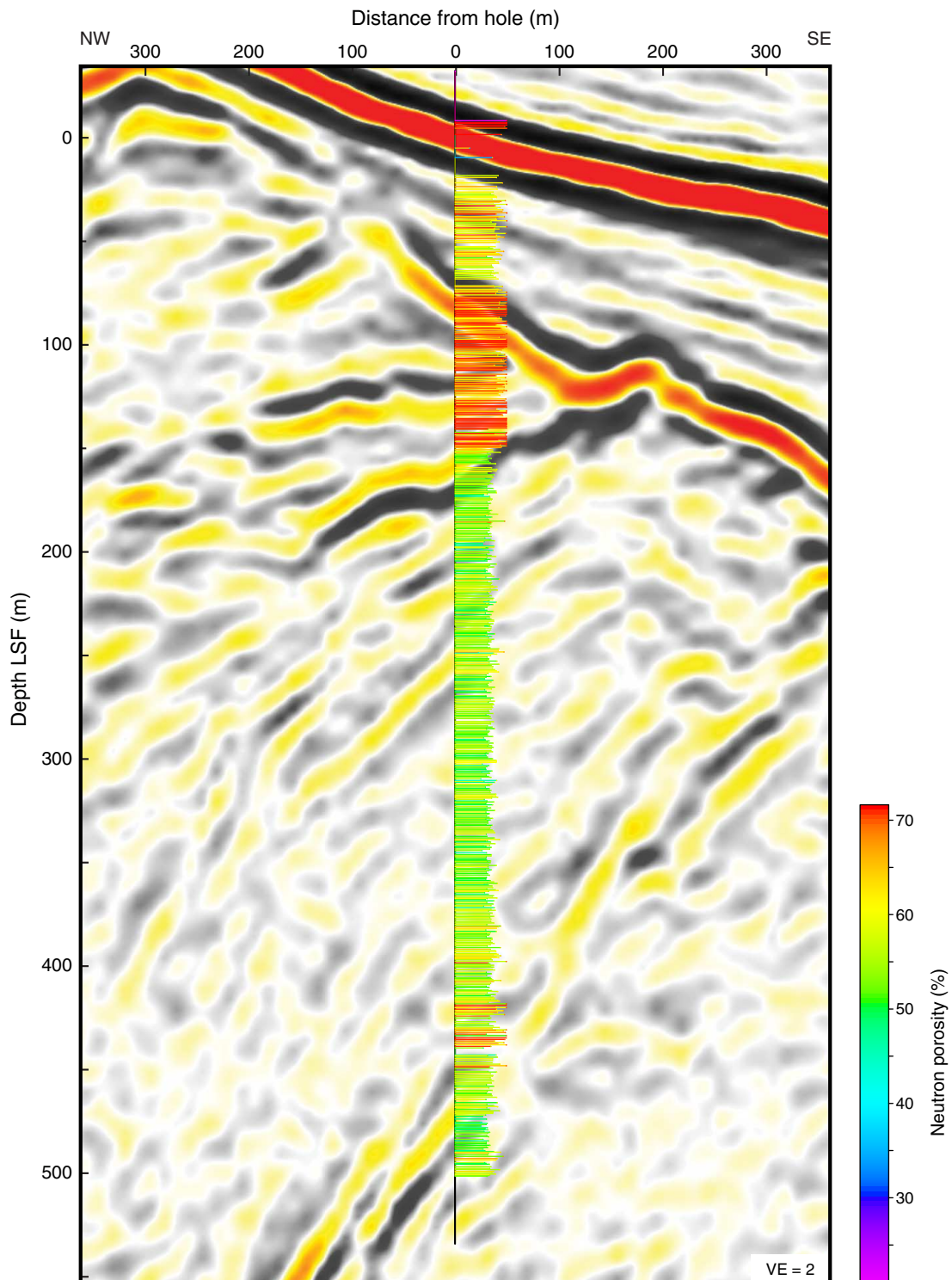


Figure F23. Real-time caliper (hole diameter) log superimposed on check shot-corrected prestack depth-migrated seismic profile through Hole C0003A. LSF = LWD depth below seafloor, VE = vertical exaggeration.

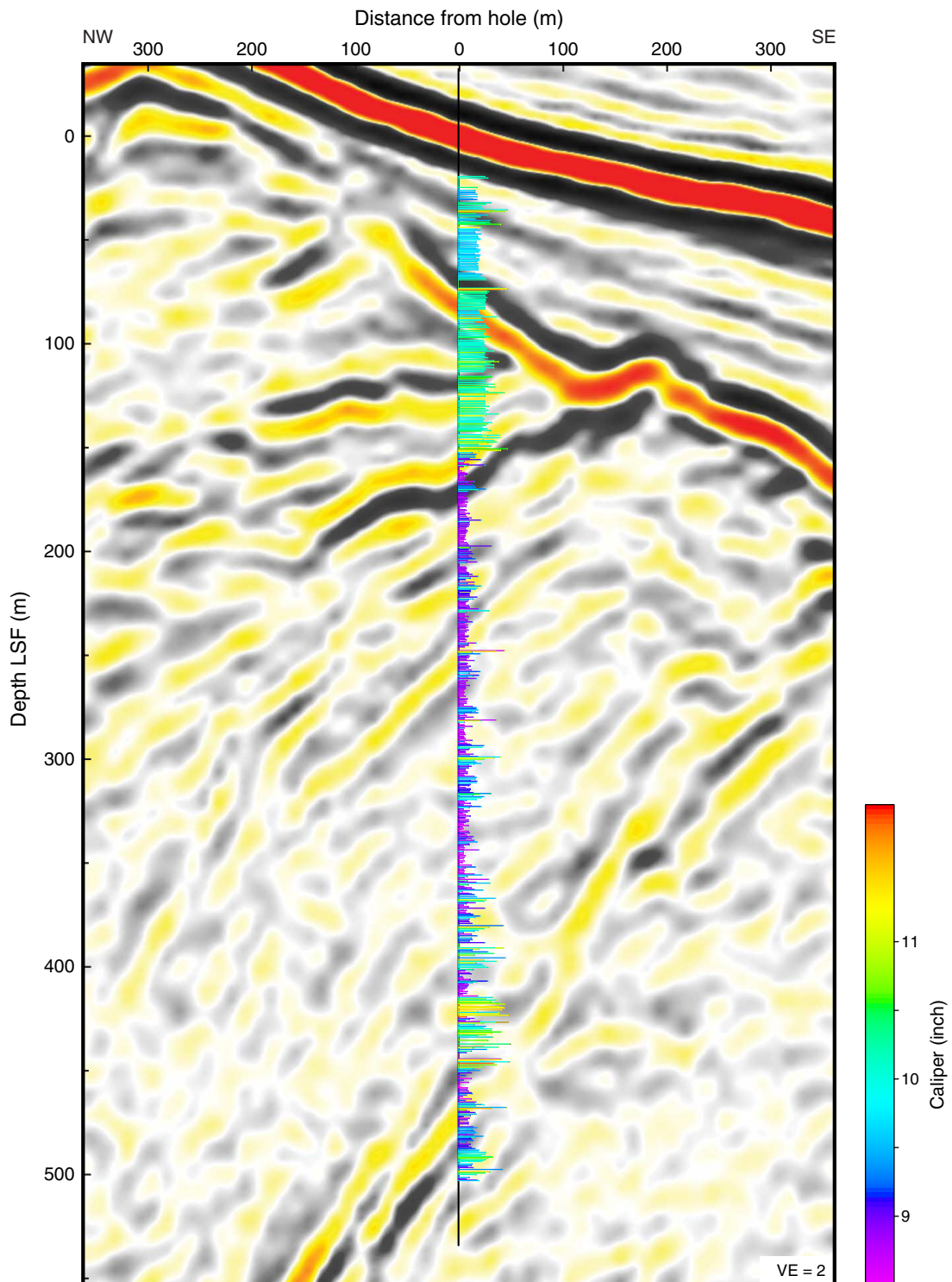


Figure F24. *P*-wave interval velocity from check shots (left) and real-time sonic log (right) superimposed on check shot–corrected prestack depth-migrated seismic profile through Hole C0003A. See “[Log-seismic correlation in zones of interest](#)” and “[Data and log quality](#)” section for important discussion of the quality of these velocity values. LSF = LWD depth below seafloor, VE = vertical exaggeration.

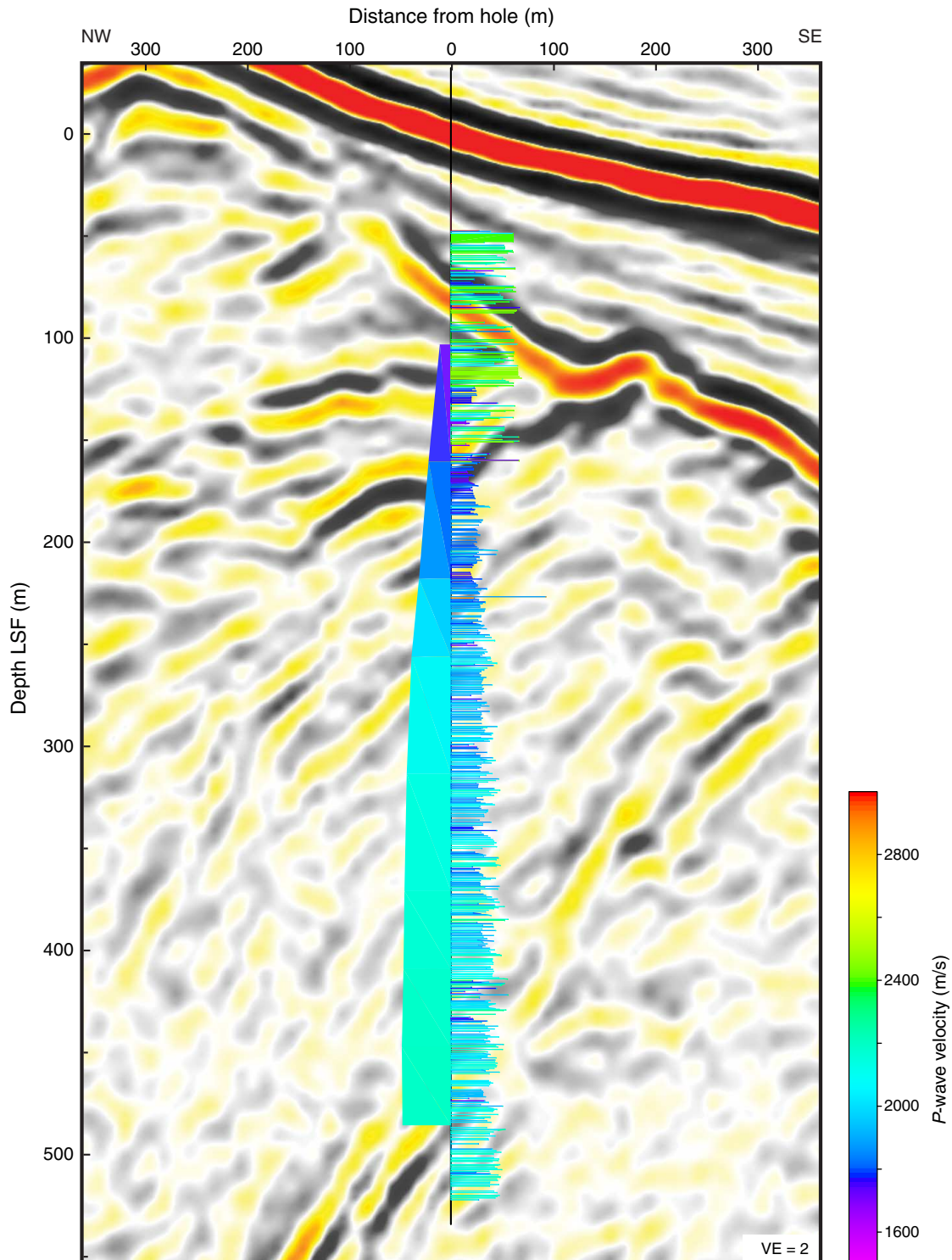


Figure F25. Seismograms from the seismicVISION tool transmitted to the surface during drilling. Each trace represents the data from one depth station. The seismograms from 15 shots to the station are stacked in the tool to create each 300 ms long trace for transmission by mud pulse to the ship. Red vertical lines = picks accepted or picked by the operator. Mud pulse system failed to transmit all or parts of the waveform for the two shallowest stations. Remaining waveforms and picks are of good quality. LSF = LWD depth below seafloor.

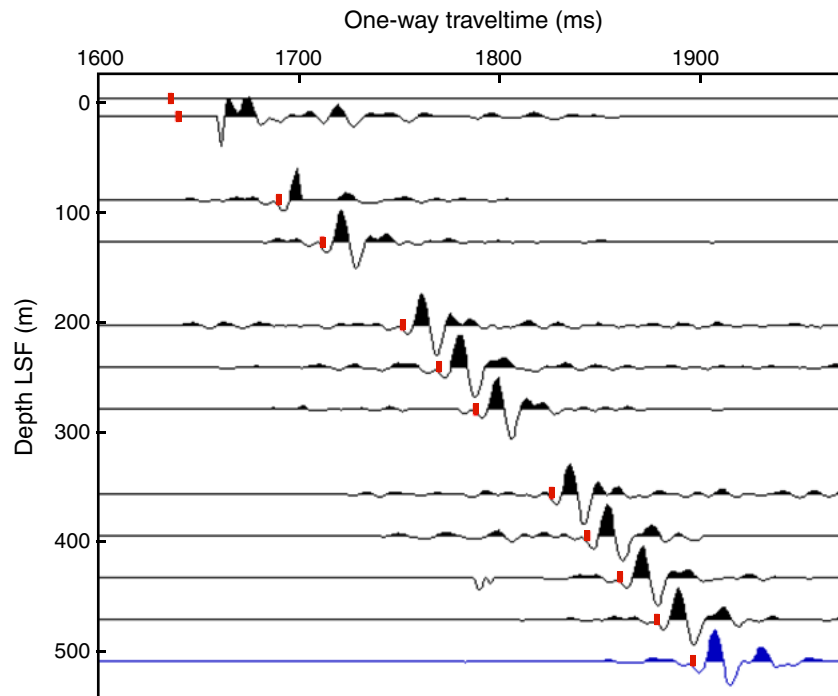


Figure F26. Smoothed check shot and real-time sonic log interval velocities. See “[Check shot survey](#)” and “[Data and log quality](#)” for discussion of the poor quality of real-time sonic picks. LSF = LWD depth below seafloor.

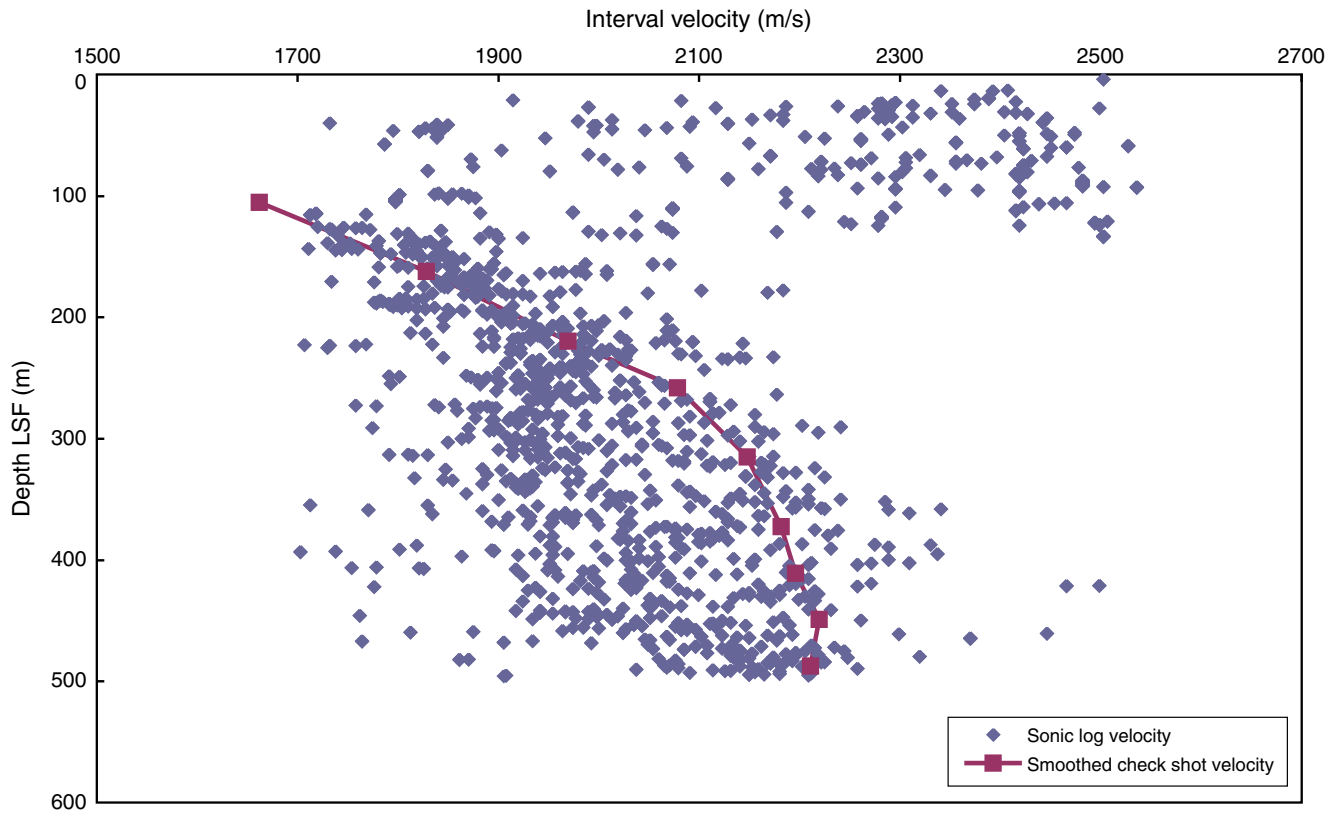




Figure F27. Seismogram modeling for Site C0003. **A.** Time vs. depth curve based on check shot. **B.** *P*-wave velocity data (see text for description). **C.** Modeled density log (see text for description). **D.** Modeled (Model.) seismogram shown as five identical traces side by side. **E.** Reflection coefficients (Refl. coeff.) determined from the input *P*-wave velocity and density data. **F.** 256 ms deterministic wavelet (Wvlt.) used for the source wavelet. **G.** Fifteen traces of depth converted inline 2595 prestack time-migrated (PSTM) section closest to borehole. **H.** Modeled seismogram repeated with positive amplitude filled in red and negative amplitude filled in blue. **I.** Fifteen traces of depth converted Inline 2595 PSTM section closest to borehole. LSF = LWD depth below seafloor, 3-D = three-dimensional.

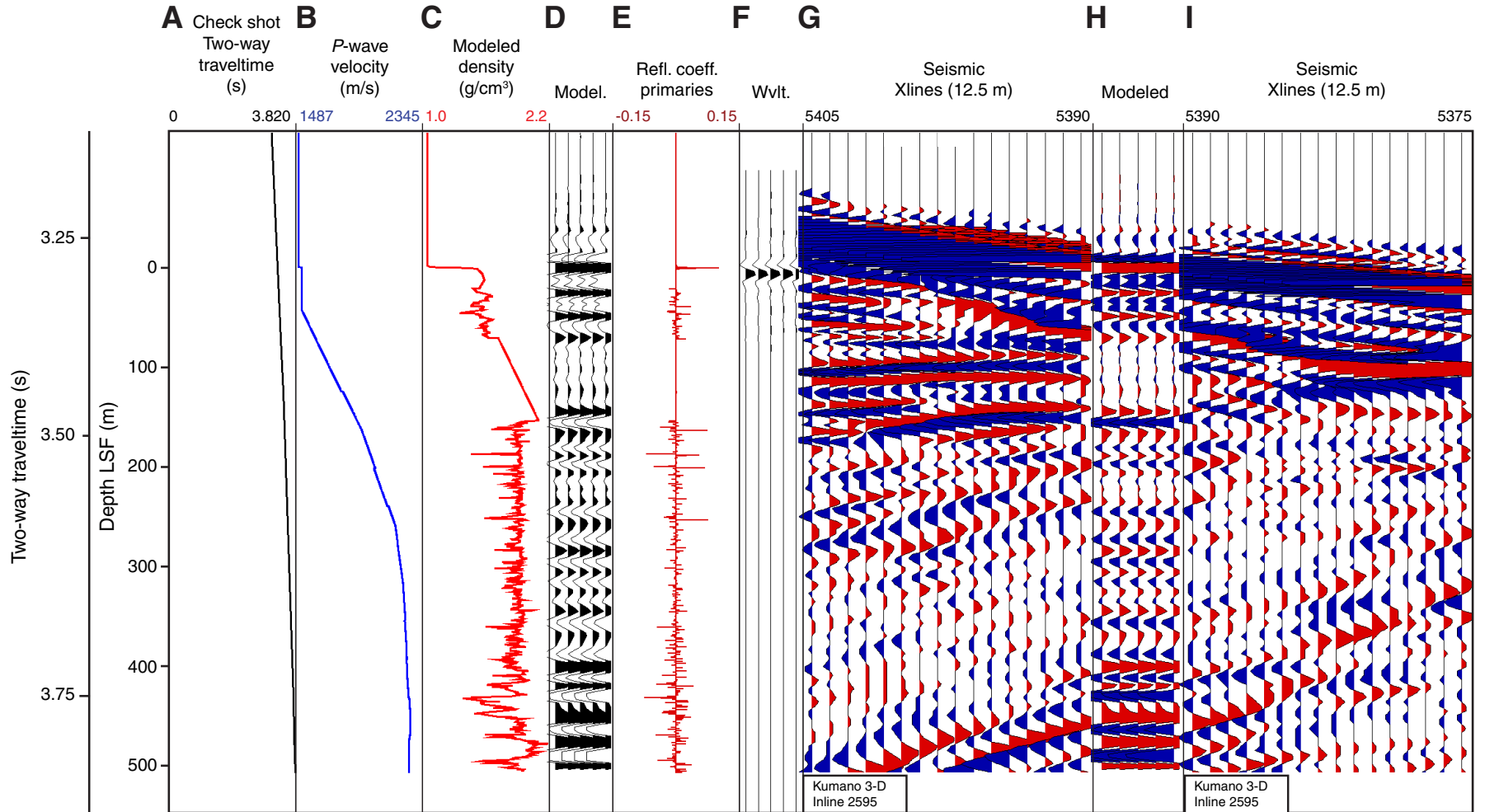


Figure F28. Interpretation of selected faults (blue) and boundary between thrust sheet and overlying slope deposits (green) in the Site C0003 region. Site C0003 likely penetrated into multiple subsidiary thrust slices of the megasplay hanging wall block. The distinction between slope deposits and thrust sheet is commonly unclear, as older slope deposits have been incorporated during ongoing thrust deformation. VE = vertical exaggeration.

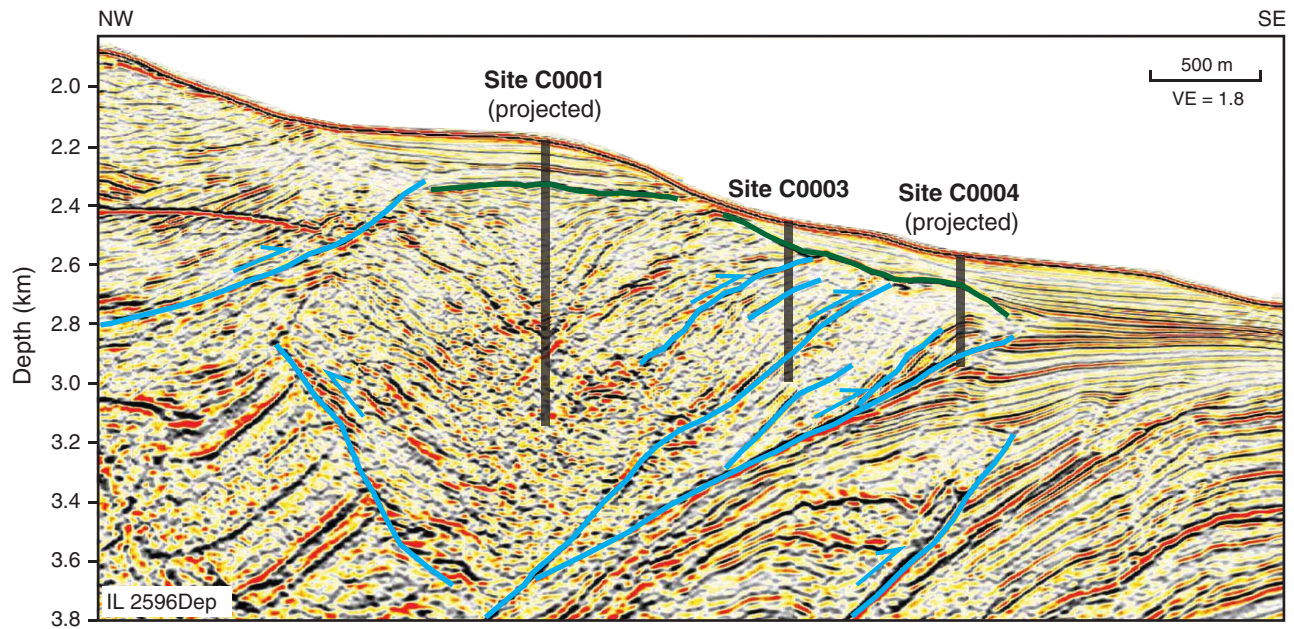


Table T1. Operations summary, Site C0003. (See table notes.)

Hole C0003A

Latitude: 33°13.3982'N

Longitude: 136°42.1382'E

Seafloor (drill pipe measurement from rig floor, m): 2481.5

Distance between rig floor and sea level (m): 28.5

Water depth (drill pipe measurement from sea level, m): 2453

Operation	Start		Depth (m LSF)		Drilled (m LSF)	Comments
	Date (Oct 2007)	Local time (h)	Top	Bottom		
Hole C0003A LWD hole	18	2200	0	525.5	533.5	8-1/2 inch LWD (GVR-sonic-SVWD-MWD-APWD-ADN).
ROV survey	20	1145				
Tag seafloor	20	1210				
Spud-in	20	1245				
Drilled depth	21	1200				
Tools stuck and packed-off	21	1000				Packed off at 3015 m DRF after pipe connection at 1000 h. Reamed and worked string between 3015 and 3006 m. Stuck in hole at 3007 m DRF at 1345 h. Failed several attempts for torque up and jar down. Pumped Hi-Vis mud to clean. Backed off while trying to turn and move the pipe at 1445 h.
Fishing and cementing Preparation	21 21	1545 1545				Made up free-fall funnel, landed on seafloor, then pulled out drill string to surface and checked the break point of assembly.
1st overshot fishing	22	1405				8-1/8 inch overshot assembly was made up, run in, reentered, washed down, and reamed from 2707 to 2785 m DRF. Attempted 7 times between 0000 and 0745 h on 24 Oct and only one was successful but failed to pull up. Pulled out at 1415 h on 24 Oct.
2nd overshot fishing	25	1415				6-3/4 inch overshot assembly was made up and run again on 25 Oct. Reentry took 10 h and the overshot failed again to catch the stuck LWD assembly. Wireline was rigged up with a 7 m sinker bar for dummy run at 2215 h on 25 Oct. After failing to pass through 2780.5 m at 0145 h on 26 Oct, the dummy tool was retrieved. Sinker bar had unscrewed and dropped off. Overshot assembly was recovered back on deck at 0000 h on 27 Oct.
3rd overshot fishing	27	0000				Made up 8-1/8 inch overshot assembly with 6-5/8 inch spiral grapple and reentered the hole at 0315 h on 28 Oct. Ran into 2774 m DRF and rigged up wireline assembly at 0600 h. Overshot latched the pipe after several attempts but failed to pass below 2788 m by wireline and rigged down. Overshot fishing continued until decision was made to pull out 1200 h of 29 Oct.
Plug and cementing	29	1200				Made up a cement stinger, run in and rigged up cement stand. Cement lines flushed at 0200 h on 30 Oct. First cement job was conducted at 0430 h and second cement job was done at 0730 h. After confirming cement return to the seabed by ROV, cementing assembly was pulled out and drill string was cleaned.

Notes: LSF = LWD depth below seafloor. LWD = logging while drilling, GVR = geoVISION resistivity tool, sonic = sonic while drilling (sonicVISION), SVWD = seismicVISION while drilling, MWD = measurement while drilling, APWD = annular pressure while drilling, ADN = Azimuthal Density Neutron tool (adnVISION). ROV = remotely operated vehicle. DRF = drillers depth below rig floor.

Table T2. Bottom-hole assembly, Hole C0003A. (See table notes.)

BHA component	Length (m)	Cumulative length from bit (m)
PDC bit	0.320	0.320
Stabilizer/float sub	1.500	1.820
Crossover sub	0.612	2.432
geoVISION	3.067	5.499
sonicVISION	7.620	13.119
Power pulse	9.025	22.144
seismicVISION	4.630	26.774
adnVISION	6.230	33.004
Crossover sub	0.610	33.614
6-3/4 inch drilling collar	9.315	42.929
6-3/4 inch drilling collar	9.319	52.248
6-3/4 inch drilling collar	9.313	61.561
6-3/4 inch drilling collar	9.315	70.876
6-3/4 inch drilling collar	9.316	80.192
6-3/4 inch drilling collar	9.313	89.505
6-3/4 inch drilling collar	9.315	98.820
6-3/4 inch drilling collar	9.314	108.134
6-3/4 inch drilling collar	9.314	117.448
6-3/4 inch drilling collar	9.318	126.766
6-3/4 inch drilling collar	9.315	136.081
6-3/4 inch drilling collar	9.314	145.395
Jar	10.212	155.607
6-3/4 inch drilling collar	9.314	164.921
6-3/4 inch drilling collar	9.314	174.235
6-3/4 inch drilling collar	9.310	183.545
6-3/4 inch drilling collar	9.310	192.855
6-3/4 inch drilling collar	9.315	202.170
6-3/4 inch drilling collar	9.310	211.480
6-3/4 inch drilling collar	9.310	220.790
6-3/4 inch drilling collar	9.315	230.105
Crossover sub	0.610	230.715
Crossover sub	0.800	231.515
Crossover sub	0.610	232.125

Notes: BHA = bottom-hole assembly. PDC = polycrystalline diamond compact.

Table T3. Logging units, Site C0003. (See table note.)

Depth (m LSF)	Logging unit	Log interpretation
55–76.6	I	Muddy to sandy and silty deposits, slope sediments
76.6–151.5	II	Sandy sediment or uncemented sandstone
151.5–509	III	Clay-rich sediment, possibly hemipelagic mud

Note: LSF = LWD depth below seafloor.

Table T4. Potential deformation-related washed out intervals in logging Unit III, Site C0003. (See table note.)

Interval depth (m LSF)	Gamma ray (gAPI)	Caliper (inch)	Ring resistivity (Ω m)
247.8–251.9	Low (62–82)	12.3	Fluctuates (1.3–2.0)
300.5–302.6	High (72–90)	11.5	Fluctuates (1.4–1.9)
381.0–383.7	Low (71–89)	12.1	Low (1.3–1.7)
392.0–402.0	High (73–103)	13.4	High (1.4–1.9)
415.7–450.5	Fluctuates (60–96)	12.7	Fluctuates (1.4–1.8)
467.7–469.6	High (77–109)	11.7	Fluctuates (1.5–1.9)

Note: LSF = LWD depth below seafloor.

Table T5. Check shot raw and smoothed traveltimes and calculated interval velocities, Site C0003. (See table notes.)

Depth* (m LSF)	Midpoint depth† (m LSF)	Raw		Smoothed	
		First arrival time* (ms)	Interval velocity† (m/s)	First arrival time* (ms)	Interval velocity† (m/s)
86.1	105.17	1694.45	1737	1692.10	1662
124.3	162.49	1716.45	1910	1715.10	1828
200.7	219.81	1756.46	2123	1756.90	1970
238.9	258.04	1774.46	2123	1776.30	2078
277.2	315.40	1792.47	2012	1794.70	2148
353.6	372.73	1830.48	2121	1830.30	2182
391.8	410.93	1848.48	2388	1847.80	2196
430.0	449.14	1864.48	2121	1865.20	2220
468.2	487.36	1882.48	2124	1882.40	2211
506.5	—	1900.49	—	1899.70	—

Notes: Smoothed values were used in the generation of synthetic seismograms and time-depth conversion of seismic reflection profiles near the site. * = first arrival time picks associated with depths of observations, † = interval velocities associated with midpoints between depths of observations. LSF = LWD depth below seafloor. — = no data.